Heft 61

# An Introduction to Air-Water Flows in Hydraulics

by Prof. Dr.
Helmut E. Kobus

Eigenverlag des Instituts für Wasserbau der Universität Stuttgart

An Introduction to Air-Water Flows in Hydraulics

by Helmut E. Kobus

**CIP Kurztitelaufnahme der Deutschen Bibliothek**

**Kobus, Helmut:**
An introduction to air-water flows in hydraulics / by Helmut E. Kobus. - Stuttgart: Inst. für Wasserbau d. Univ., 1985.
(Mitteilungen / Institut für Wasserbau der Universität Stuttgart; Heft Nr. 61)
ISBN 3-921694-61-2

NE: Institut für Wasserbau <Stuttgart>: Mitteilungen



Herausgegeben 1985 vom Eigenverlag des Instituts für Wasserbau

| | | |
|---|---|---|
| Druck: | Sprint-Druck, | Stuttgart |
| Umschlag: | Entwurf | Monika Kuschel |
| | Photo | Uwe Hagemann |
| | Herstellung | Industriedruck Stuttgart |

# VORWORT

Das vorliegende Mitteilungsheft wurde als Beitrag zu dem im Entstehen begriffenen HYDRAULIC STRUCTURES DESIGN MANUAL der IAHR (International Association for Hydraulic Research) verfaßt. In diesem Rahmen soll eine Reihe von Monographien entstehen, in denen die hydraulischen Entwurfsgrundlagen für Wasserbauwerke zusammengestellt werden. Im September 1984 wurde ich anläßlich des IAHR-Symposiums in Esslingen zum Thema "Scale Effects in Modelling Hydraulic Structures" gebeten, einen Grundlagenbeitrag zum Thema Wasser-Luft-Gemische beizusteuern. Aus diesem Anlaß entstand der vorliegende Beitrag in englischer Sprache.

In der Monographieserie werden Wasser-Luft-Gemische sowohl in Heft A5 (Air-water flow in open channels) als auch in Heft A12 (Air-water flow in closed conduits) behandelt. Mein Beitrag gibt im ersten Teil eine allgemeine Einführung zum Gesamtthema und behandelt dann den örtlichen Lufteintrag in Gerinneströmungen. Er soll deshalb im Rahmen der Monographie A5 zusammen mit Beiträgen von I. Wood (Neuseeland), P. Volkart (Schweiz) und N.S. Pinto (Brasilien) erscheinen.

Viele wertvolle Anregungen verdanke ich I. Wood, der den Entwurf einer sorgfältigen kritischen Durchsicht unterzogen hat. Ihm gilt mein besonderer Dank ebenso wie H.-P. Koschitzky, der mich bei der Ausarbeitung des Beitrags tatkräftig unterstützt hat. Des weiteren bin ich A. Ervine (Großbritannien) für seine konstruktiven und hilfreichen Kommentare dankbar. Schließlich habe ich I. Wood und N. Thomas (Großbritannien) für die Überlassung von Fotoaufnahmen zu danken.

Der vorliegende Beitrag ist als allgemeine Einführung in das schwierige Thema der Wasser-Luft-Gemische im Wasserbau gedacht. Als Baustein zu der Monographieserie soll er zur systematischen Orientierung beitragen und sowohl die heute verfügbaren Entwurfsgrundlagen als auch die noch vorhandenen Wissenslücken aufzeigen. Es ist zu hoffen, daß dieser Zweck erfüllt werden kann.

Stuttgart, im Oktober 1985 Helmut Kobus

# PREFACE

This report has been written as a contribution to the HYDRAULIC STRUCTURES DESIGN MANUAL, which is in preparation by the International Association for Hydraulic Research (IAHR). Within this framework, a series of monographs is being planned, in which the hydraulic design criteria for civil engineering structures are to be collected. In September 1984, on the occasion of the IAHR-Symposium in Esslingen on "Scale Effects in Modelling Hydraulic Structures", I was asked to participate in these efforts with a basic contribution on the topic of air-water mixtures. For this reason, the present report has been prepared in English language.

In the monograph series, air-water mixtures will be treated both in volume A5 (Air-water flow in open channels) and in volume A12 (Air-water flow in closed conduits). My contribution contains in the first part a general introduction to the entire topic and then treats local air entrainment processes in open channel flows. It is therefore intended to appear within monograph A5, together with contributions by I. Wood (New Zealand), P. Volkart (Switzerland) and N.S. Pinto (Brazil).

Many valuable suggestions I owe to I. Wood, who has reviewed the draft thoroughly and critically. I owe particular thanks to him as well as to H.-P. Koschitzky, who gave me his active support in the preparation of the report. Furthermore, I am indebted to A. Ervine (Great Britain) for his pertinent and helpful comments. Finally, I gratefully acknowledge that a number of photographs have been supplied by I. Wood and N. Thomas (Great Britain).

The present contribution is intended as a general introduction to the difficult topic of air-water mixtures in hydraulic engineering. As an element in the monograph series, it is intended to contribute to a systematic orientation and to indicate both the presently available design criteria and the still existing gaps of knowledge. It is hoped that this purpose can be achieved.

Stuttgart, October 1985 Helmut Kobus

CONTENTS

LIST OF FIGURES

LIST OF SYMBOLS

| | | |
|---|---|---|
| $b,B$ | [m] | width |
| $c_a$ | [%] | air concentration |
| $c_d$ | [-] | drag coefficient (resistance coefficient) $c_d \equiv \frac{4g \cdot d_b}{3 v_b^2}$ |
| $c_{pe}$ | [-] | pressure coefficient $c_{pe} \equiv \frac{\Delta p_e}{\rho_w v_w^2/2}$ |
| $D,d$ | [m] | diameter |
| $d_b$ | [m] | equivalent bubble diameter (sphere of equal volume) |
| $d_n$ | [m] | nozzle diameter |
| $d_o$ | [m] | orifice diameter |
| $d_p$ | [m] | plunge pool depth |
| $\Delta E$ | [m] | energy head loss due to hydraulic jump |
| $F_B$ | [N] | buoyancy force |
| $F(v_b)$ | [N] | resistance force to the slip velocity |
| $Fr$ | [-] | Froude number $Fr \equiv \frac{v_w}{\sqrt{g\, l_w}}$ |
| $g$ | [m/s$^2$] | gravitational acceleration |
| $h$ | [m] | height of fall |
| $\Delta h$ | [m] | piezometric head difference |
| $k_r,k_1$ | [-] | coefficients |
| $k_e$ | [-] | entrainment coefficient |
| $l_e$ | [-] | boundary length scale |
| $l_w$ | [m] | reference length |
| $L_o$ | [m] | jet break-up length |
| $l_t$ | [-] | turbulence length scale |
| $M_{w,z}$ | [N] | vertical momentum flux |
| $p$ | [Pa] | pressure |
| $\Delta p_e$ | [Pa] | pressure difference |
| $p_o$ | [Pa] | atmospheric pressure |
| $Q_a$ | [m$^3$/s] | air discharge |
| $q_a$ | [m$^2$/s] | specific flow rate (air) per unit width |

| | | |
|---|---|---|
| $Q_{ae}$ | [$m^3/s$] | total rate of entrained air |
| $q_{ae}$ | [$m^2/s$] | specific rate of entrained air per unit width |
| $Q_{at}$ | [$m^3/s$] | total air transport rate |
| $q_{at}$ | [$m^2/s$] | specific air transport rate per unit width |
| $q_j$ | [$m^2/s$] | jet discharge per unit jet perimeter |
| $q_t$ | [$m^2/s$] | net air transport |
| $Q_w$ | [$m^3/s$] | water discharge |
| $q_w$ | [$m^2/s$] | specific water discharge per unit width |
| r | [%] | reoxigenation rate |
| R | [m] | hydraulic radius of the jet at impact |
| Re | [-] | Reynolds number $Re \equiv \frac{v_b d_b}{\mu_w/\rho_w}$ |
| $Re_t$ | [-] | minimum Reynolds number for fully turbulent flow |
| s | [m] | distance between slots |
| Tu | [-] | turbulence characteristics |
| $v_b$ | [m/s] | bubble rise velocity |
| $v_c$ | [m/s] | critical velocity |
| $v_e$ | [m/s] | velocity at the line of air entrainment, impingment velocity |
| $v_H$ | [m/s] | cross flow velocity |
| $v_t$ | [m/s] | turbulent fluctuations RMS |
| $v_w$ | [m/s] | water velocity |
| We | [-] | Weber number $We \equiv \frac{v_w}{\sqrt{\sigma_{wa}/\rho_w \cdot l_w}}$ |
| y | [m] | water depth |
| $y_1$ | [m] | inflow water depth upstream of the hydraulic jump |
| Z | [-] | liquid parameter $Z \equiv \frac{g \cdot \mu_w^4}{\rho_w \cdot \sigma_{wa}^3}$ |
| $\beta_e$ | [%] | relative air entrainment $\beta_e \equiv q_{ae}/q_w$ |
| $\gamma_w$ | [$kN/m^3$] | specific weight |
| $\rho_a$ | [$kg/m^3$] | density of air |
| $\rho_w$ | [$kg/m^3$] | density of the liquid |
| $\mu_w$ | [kg/ms] | dynamic viscosity of the liquid |
| $\nu_w$ | [$m^2/s$] | kinematic viscosity of the liquid |
| $\sigma_{wa}$ | [N/m] | surface tension at the liquid-gas interface |

# 1. INTRODUCTION TO AIR-WATER FLOWS

## 1.1 General types of air-water flows

For many hydraulic structures, safe operation can only be achieved if not only the characteristics of the water flow are considered, but due attention is given to the simultaneous movement of air in the system. The difference in specific weight of air and water is large, so that they are usually well separated by a sharp interface. However, a number of flow configurations lead to an intensive mixing across this surface. This is called air entrainment. Consideration of the effects of the entrained air upon the water flow may be essential for the safe operation of a hydraulic structure.

There is a great variety of flow configurations in which the air flow may affect the water flow. We can distinguish:

### 1.1.1 Air demand in hydraulic structures without mixing.

In order to maintain reasonable pressures in closed hydraulic systems, air is often allowed to enter the system, and where it accumulates it is released from the system. Basically, there are two configurations:

- Air flow to a finite-volume air chamber due to a falling or rising water surface affecting the chamber volume. For the design of adequate aeration devices, the resulting air demand can usually be computed in a straight- forward manner.
- Air demand in closed conduits flowing partially full. The drag of the moving water surface generates an air flow which has to be accounted for at the intake (often requiring air vents) and at the outlet. For known water flow velocities, usually a reasonable estimate of the air demand can be obtained.

### 1.1.2 Air entrainment in hydraulic structures (air demand with mixing)

The complex two-phase flow resulting from the entrainment and

transport of air bubbles is the subject of this monograph. The process which forces air through a surface into a water volume is called entrainment; the process of bubble escape from the surface is called detrainment. There are many flow situations causing entrainment. The supply of air may be:

- unlimited (air supply from the atmosphere); or
- a limited air supply from an air chamber, which may or may not be connected to the atmosphere by an air duct. In this case, there is an interaction between air flow, air pressure in the system and water flow.

The region of detrainment is not necessarily near the entrainment point; depending upon the water flow conditions and their transport capacity, the air may be transported over large distances to the region of detrainment (Fig. 1.1). Here also one has to distinguish:

- unlimited air escape to the atmosphere;
- limited air escape in closed systems, leading to air accumulations in certain regions such as high points or along the top of conduits. These air pockets can decrease the water discharge and thus have a direct feedback upon the water flow.

The major flow configurations leading to air entrainment in hydraulic structures will be described in more detail in section 1.2

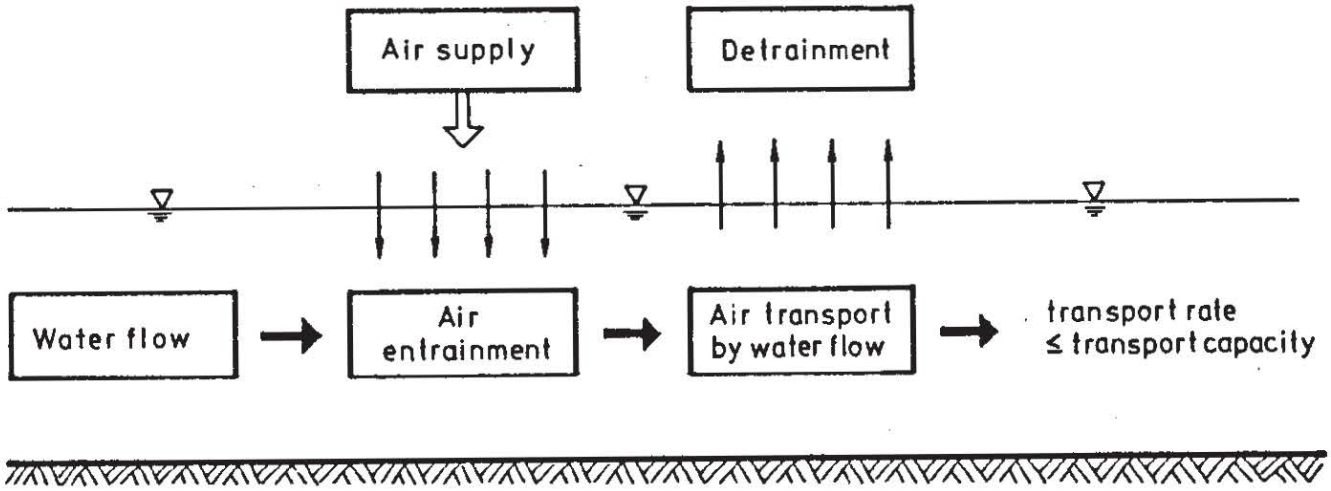


Fig. 1.1: Air entrainment, detrainment and transport

### 1.1.3 Formation of air-water mixtures by air coming out of solution.

The saturation concentration for dissolved oxygen and nitrogen in water varies considerably with the pressure and the temperature of the water. Therefore, in closed-conduit systems it may happen that pressure and/or temperature changes cause formation of small gas bubbles in the interior of the liquid. Since the elastic properties and the wave propagation speed vary drastically with the presence of gas bubbles even at very low concentrations, this phenomenon is of considerable importance in the design of closed conduit systems, particularly with respect to fast changes in flow (hydraulic transients). These phenomena will be treated in monograph A-12 ("Air-water flow in closed conduits") and hence are excluded here.

### 1.1.4 Designed aeration systems.

Designed aeration systems of various kinds are employed mainly for the purpose of reoxygenation of polluted water. They are primarily installed in sewage treatment plants and in polluted rivers and lakes for water quality enhancement. The various technical devices operate essentially on two principles:

- Formation of an air-water mixture at a surface: surface rotors, spray devices or water jet pumps, either use external energy or else part of the flow energy (thus contributing a considerable local energy loss) in order to force air into the water.
- Formation of an air-water mixture by injecting air beneath the surface: submerged nozzles, perforated tubes or porous filter plates are employed for the dispersion of compressed air in the water. In sewage treatment, the injected air serves the dual purpose of providing oxygen to the water and, by the action of the bubbles, producing a water flow with increased mixing. Similar systems are employed in natural rivers and lakes as active means to improve the water quality. Such bubble plumes also find applications as pneumatic oil barriers, vertical mixers for density currents, devices for combatting formation

of an ice cover or for damping underwater detonation waves, etc. A detailed treatment including design information for such systems is given in (Kobus, 1973).

Designed aeration systems are not treated in this monograph.

## 1.2 Types of aeration and processes of entrainment in hydraulic structures

Flow conditions which cause air entrainment, i.e. transport of air through a free water surface, may be termed "self-aerating", giving rise to "surface aeration" or else "natural aeration". Quite generally, we can distinguish flows where entrainment takes place all along the water surface (ambient aeration) and flows where entrainment occurs locally at a surface discontinuity (local aeration). The following processes can be distinguished:

### 1.2.1 Surface aeration in high-speed flows

In high-speed open channels flows like in spillways or chutes, the flow turbulence gives rise to surface disturbances leading to air entrainment. Similarly, high-speed free jet flows generated by fire monitors, hollow jet valves, or flip bucket ejectors, etc. experience surface disturbances due to the initial jet flow turbulence and the shear forces of the surrounding air. These disturbances grow and lead to air entrainment along the jet surface and in many cases to a complete desintegration of the jet.

Fig. 1.2 is a photograph of the surface of a high-speed flow down a spillway. In this case, the effects of a multitude of irregular high-energy vortices result in the contorted three dimensional nature of the surface. Through this surface, air is continually being trapped and escaping. The major entraining mechanisms in this case consist of overturning surface waves and of water droplets being projected above the water surface and then falling back. In penetrating the water surface, they drag air into the water. This process was suggested by Lane (1939), Rajaratnam (1962) and Hino (1961). It has been demonstrated in some classic experiments by Volkart (1980). However, undoubtedly the mechanism of air entrapment in vortices as described below also contributes to the entrainment at the surface. The mixing zone of air and water extends into the clear water region and may extend to the channel bottom.

Fig. 1.2: Surface aeration in high-speed flow (Surface of the air entraining region on Aviemore Spillway. Photo: I. Wood, 1984)

1.2.2 Local aeration by impinging jets

Free-surface flow configurations leading to local air entrainment are always connected with some form of surface discontinuity. A number of jet-type flow configurations is sketched in Fig. 1.3.

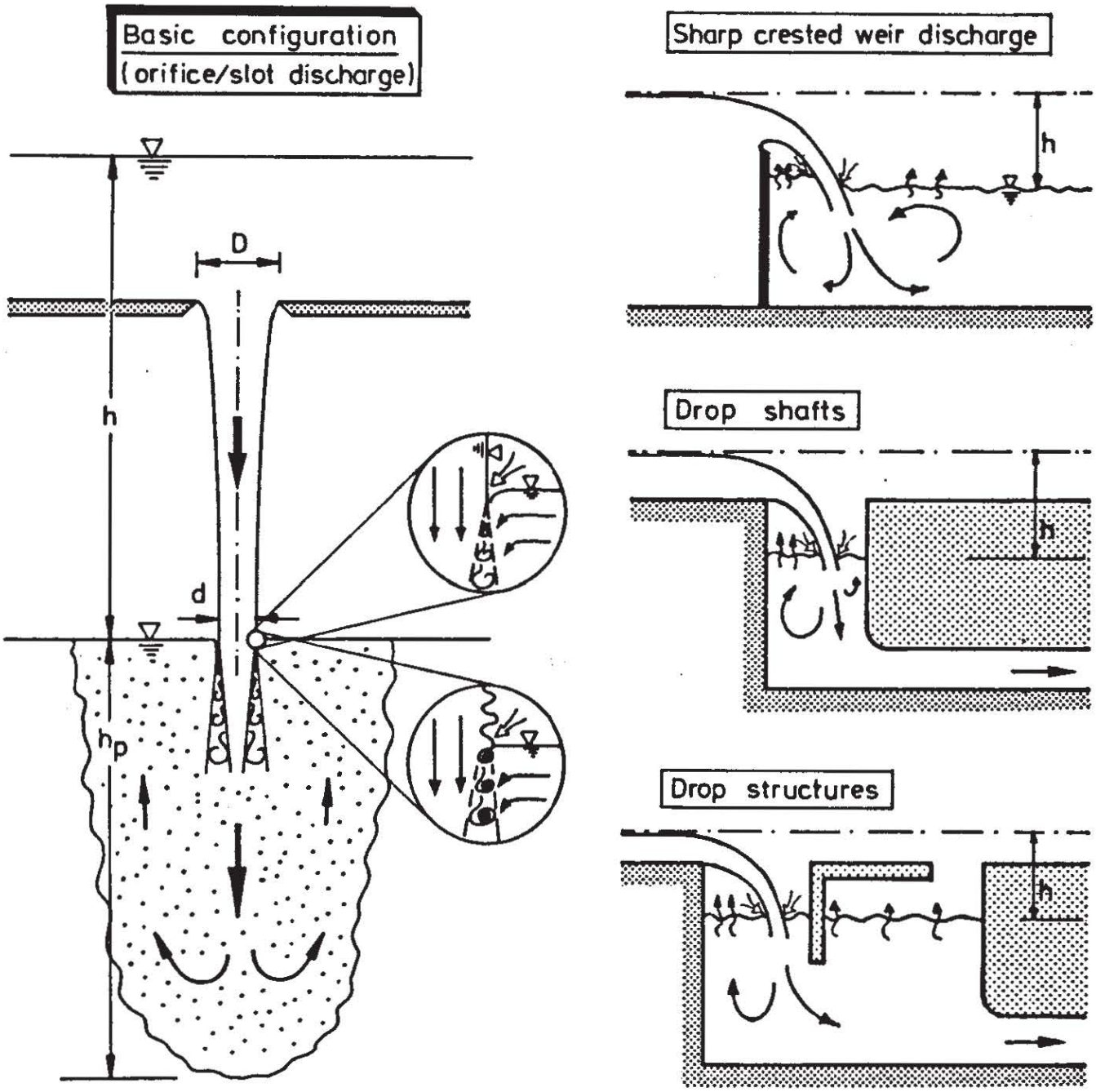


Fig. 1.3: Local air entrainment at "plunging-jet type" configurations

These include sharp-crested weirs, free overfalls and drop structures. These flows differ from ambient surface aeration by the fact that in local aeration processes air may be entrained at a rate completely independent of the transport capacity of the flow. The transport capacity only determines the distance over which the suspended air is transported. If the transport capacity of the flow is low, therefore, the entrained air will be rather quickly escaping into the atmosphere again, and the process of self-aeration will be of local importance only. An example of this local aeration process gives Fig. 1.4.

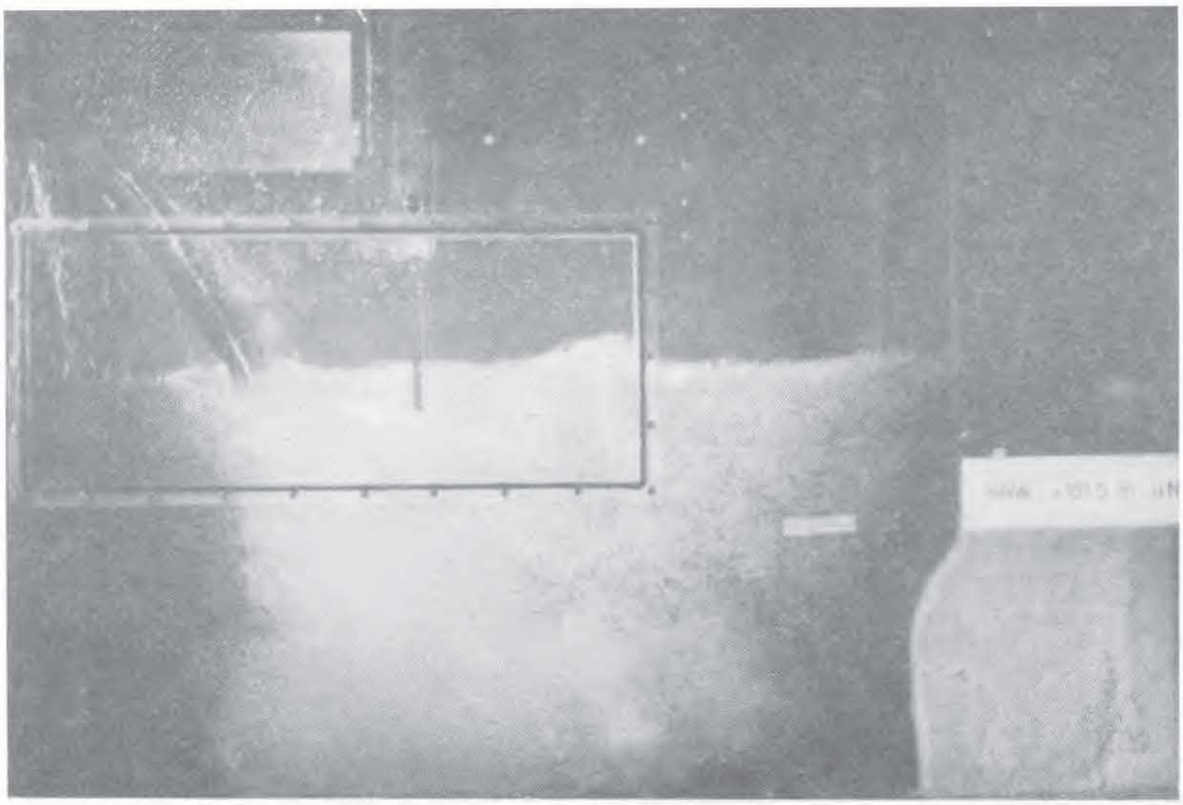

Fig. 1.4: Air entrainment in a plunging free jet

Flow configurations of the plunging-jet type are characterized by the fact that local air entrainment takes place at the intersection of the free jet with the water surface. The momentum of the water jet causes the air to be entrained in the highly turbulent shear layer induced by the jet surface. Fig. 1.5 illustrates that the entrainment takes place mainly in relatively

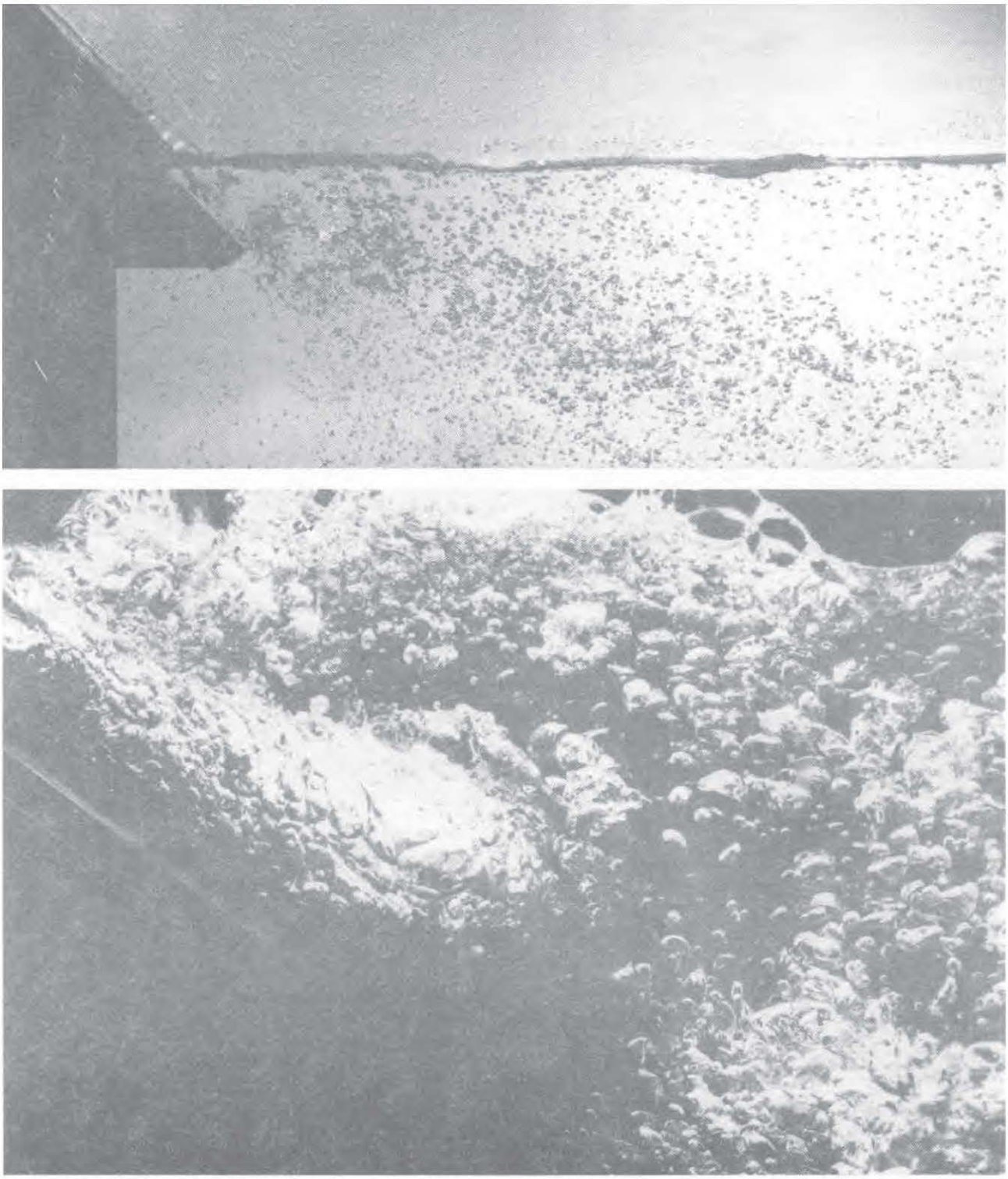

Fig. 1.5: Air entrainment in a supported inclined jet by vortices with axes perpendicular to the flow direction
(a) overall view (Photo: I. Wood, 1984)
(b) close-up of foam layer and vortex (Photo: N. Thomas in Goldring et al, 1980)

distinct vortices with longitudinal axes nominally perpendicular to the flow direction. Thomas (1978) suggested that the vortices in the intensive shear layer at the penetration point are sufficiently strong to entrain air in the vortex cores. This entrainment may be enhanced by the development of turbulence on the jet surface prior to its contact with the free surface (Ervine, 1976) and/or by the formation of a foam layer on the free surface.

In plunging-jet configurations, the momentum flux of the jet is predominantly in the vertical downward direction. The vertical momentum flux input will be directly counteracted by the buoyancy force of the entrained air, whereas the horizontal momentum flux components will remain essentially unchanged, since they experience no external force.

1.2.3 Local aeration in hydraulic jump configurations

Another surface- and velocity discontinuity causing air entrainment is observed at the toe of a hydraulic jump, as it is typically encountered downstream of control structures and in stilling basins. Related to this is the air entrainment in moving hydraulic jumps (surge waves) or even in the unsteady breaking of shallow water waves, which engulf much air in the process. Also, jets impinging on rigid walls (e.g. in selfpriming configurations for siphons) produce a surface roller with self aeration resembling the hydraulic jump configuration.

Fig. 1.6 shows flow configurations of the surface roller type, which are encountered most frequently in nearly horizontal flows. Fig. 1.7, shows that the local air entrainment at the toe of the surface roller occurs much in the same manner as in the plunging jet. Again, the air is entrained into the free shear layer which is characterized by intensive turbulence production, predominantly in vortices with axes perpendicular to the flow.

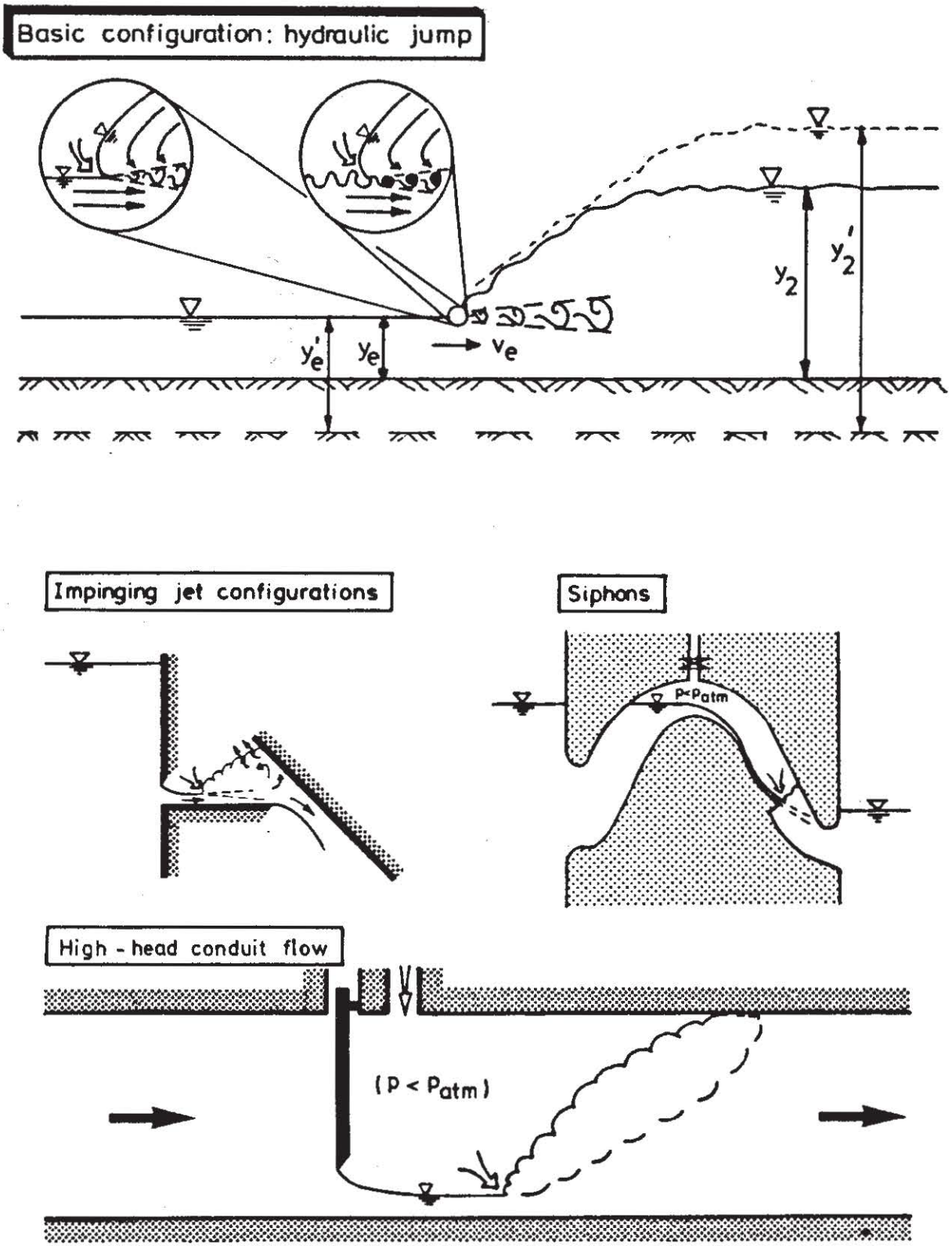


Fig. 1.6: Local air entrainment at "surface-roller type" configurations

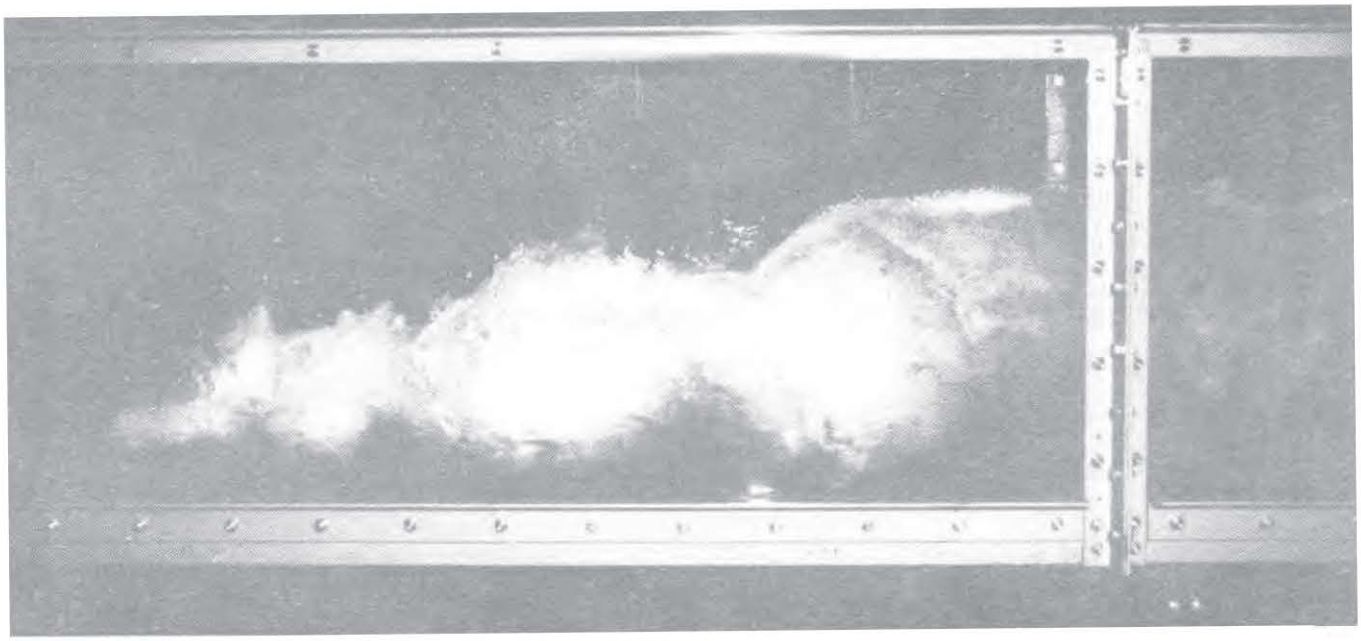

Fig. 1.7: Air entrainment in a hydraulic jump by vortices at the toe with axes perpendicular to the flow direction (Photo: B. Barcewski, 1985)

The entire flow field including the surface roller is governed by the momentum flux of the approach flow and by the downstream boundary condition. For a given flow configuration, the Froude number of the approach flow determines the downstream water depth and hence also the geometry and intensity of the surface roller.

### 1.2.4 Local aeration in the wake of bluff bodies

Zones of flow separation in the wake of bluff bodies or at abrupt expansions of the cross section are characterized by a significantly lower pressure level as compared to the main flow. For bluff bodies protruding through the water surface, this leads to a marked surface depression in the separation zone. The line of flow separation penetrates the water surface. The intensive turbulence in the free shear layer leads to vortex formation (vortex axis perpendicular to flow) which may cause local air entrainment into the vortex cores. It is often observed that air

entrainment is particularly pronounced near the channel side walls due to such effects on wall protrusions. Also, stilling basin blocks, piers or large rocks in fast flows exhibit this characteristic quite clearly.

The action of bottom offsets in spillways or conduits can be approximately related to this type of air entrainment. However, the situation differs in three ways:

- the line of flow separation is horizontal along the inclined bottom, rather than vertical and protruding through the water surface;
- the air supply is not directly from the atmosphere, but through an air duct system.
- air is entrained into the water upward from below, rather than downward from above as in all other configurations.

### 1.2.5 Local aeration at transitions from free-surface to conduit flow

Transitions from free-surface to conduit flow are encountered at intake structures, pump sumps, control structures, gates, drop shaft spillways, etc. Upstream from the transition to pressurized flow, there results a region of stagnation at the water surface, and depending upon the approach flow and boundary geometry, swirl and vortex formation may lead to air entrainment into the system.

In this case, air is entrained by distinct vortices with axes parallel to the flow direction. The major mechanism is the stretching of patches of environmental vorticity until the rotation of the core becomes sufficiently large and consequently the pressures sufficiently small for air to be drawn into the core. Fig. 1.8 shows the flow under a sluice gate where such a vortex with air in its core is apparent.

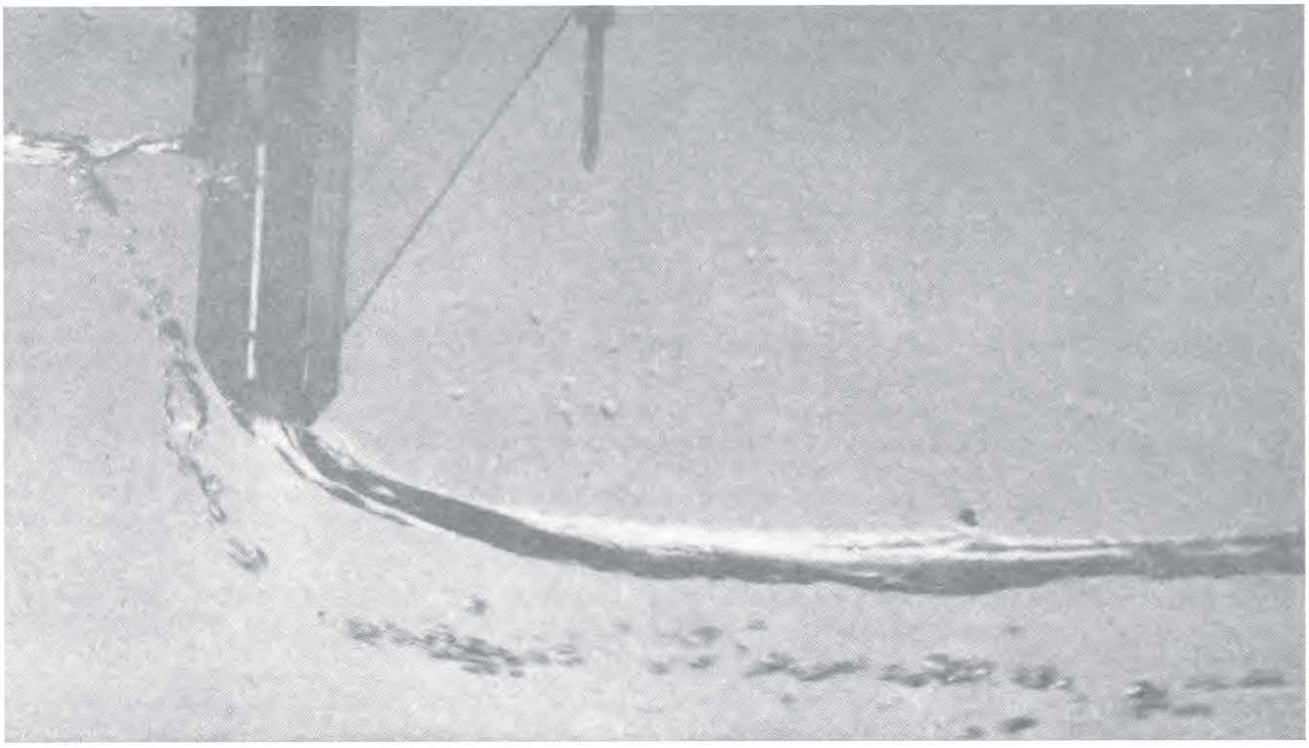

Fig. 1.8: Air entrainment at a sluice gate by a vortex with an axis parallel to the flow. Similar flow conditions are encountered at intake structures. The vortex develops from the environmental vorticity in the approach flow (Photo: I. Wood, 1984)

Air entrainment into closed-conduit systems is usually most undesirable for a number of reasons, such as disturbances of pump performance or flow variations due to the detrainment and accumulation of air in the system. For further information on this distinctly different type of air entrainment, the reader is referred to monographs A-6 "Swirl-Flow Problems at Intakes" and A-12 "Air-Water Flow in Closed Conduits".

## 1.3 Effects of entrained air upon the water flow

Entrained air can strongly influence the performance of hydraulic structures for the following reasons:

- The bulk properties of the fluid (mixture of air and water) are changed. This concerns mainly the density and the elasticity.
- The presence of air changes the structure of flow turbulence (possibly including wall shear).
- The presence of air helps to avoid excessive negative pressures and cavitation.
- Air bubbles introduce vertical momentum into the flow due to their buoyancy. This may have significant effects upon the flow field.
- In open channels, entrained air leads to an increase in water depth (bulking).
- In closed conduits, for a given flow cross section the presence of air leads to changes in water discharge or pressure distribution in the system.
- The presence of air affects the performance of hydraulic machinery adversely.
- In hydraulic transients, pressure waves are strongly damped and deformed.
- Air accumulating in a system may lead to disruption of the flow and such effects as "blow-out" or "blow-back";
- The presence of air bubbles leads to an intensive oxygen and nitrogen transfer until the surrounding water has reached saturation.

Air entrainment is in some cases desirable and in others undesirable. It is desirable, e.g. for cavitation prevention, for oxygenation purposes or damping effects in hydraulic transients; undesirable examples include effects on pumps, on intake structures and on closed conduit systems.

## 1.4 The role of the transport capacity

A self-aerating flow configuration continuously produces air bubbles by mechanical action, which are subsequently carried away by the flow, if the transport capacity of the water flow is sufficiently high. All those bubbles which are entrained but cannot be transported by the flow will escape through the water surface (detrainment). This illustrates the interaction of air entrainment, transport capacity and detrainment. For a given configuration, the air entrainment is governed by the upstream conditons, whereas the transport capacity depends entirely upon the downstream water flow configuration. If the transport capacity is zero (as e.g. in stagnant or slowly flowing water bodies), then all entrained air will be detrained.

The transport capacity of the water flow depends primarily upon the ratio between water velocity $v_w$ and bubble rise velocity $v_b$. In stagnant water bodies ($v_w << v_b$), the transport capacity is zero. The air bubbles will rise due to their buoyancy to the surface and escape. In slowly flowing water ($v_w \approx v_b$), the entrained air bubbles are displaced by the water flow, while the flow field may be changed drastically by the air bubbles.

In open channel high-speed flows ($v_w \gg v_b$), the transport capacity increases with increasing velocity (i.e. channel slope) and turbulence intensity of the water flow. The transport capacity is characterized by an equilibrium situation between the rising tendency of the bubbles and the counteracting mixing effect of the turbulent fluctuations in a concentration gradient, quite analog to the transport of suspended solids (although bubbles do show several distinct differences to solid particles).

In closed conduit flow, the transport capacity is additionally dependent upon the orientation of the flow with respect to the direction of the buoyancy force. In plane flows, buoyancy will usually act in the vertical direction. Obviously, the transport

capacity will be a maximum in vertically upward flow and a minimum for vertically downward flow.

Whenever the local air entrainment exceeds the transport capacity of the subsequent channel or conduit, detrainment will take place. The resulting net detrainment can be expected to be proportional to the excess amount of air exceeding the transport capacity. A hydraulic jump, for instance, entrains a considerable amount of air locally, but because of little or no air transport capacity discharges most of it back into the atmosphere through the surface roller, so that after a short distance downstream the air content of the flow is almost zero again.

If the transport capacity is exceeded in conduit flows, then the "detraining" air will collect at the top of the conduit and form air pockets of increasing size. Depending upon the flow velocity and the inclination of the conduit, these pockets, after they have reached a certain size, may move in the direction of flow or against it. This results in unsteady flow conditions with considerable pressure fluctuations and flow instabilities in the system ("blowout" or "blowback").

## 1.5 Parameters for air-water flows in open channels

For open channel flows as discussed in this monograph, there exists

- always unlimited air escape directly to the atmosphere;
- usually also unlimited air supply directly from the atmosphere (with the exception of spillway aerators or weir aeration);
- a direct dependence of the transport capacity upon the characteristics of the open channel flow.

This excludes a priori any effects of independent variation of flow inclination or of limited air escape with feedback upon the flow, as it may be encountered in pressurized flow in closed conduits. These aspects will be treated in monograph A-12.

The dependent variables describing the air entrainment, transport and detrainment process are air flow rates $Q_a$ resp. $q_a$, resulting bubble sizes $d_b$, air concentrations $c_a$ and bulk dimensions of the air-water mixture, as well as trajectories and residence times of bubbles. In air flow rates, we have to distinguish

- the total rate of entrained air, $Q_{ae}$
- the specific rate of entrained air (per unit width) $q_{ae}$

and in contrast to these

- the total air transport rate $Q_{at}$
- the specific air transport rate $q_{at}$.

All of the dependent variables can be described in terms of independent variables representing

- boundary geometry: reference length $l_w$; geometric lengths;
- water approach flow: reference velocity $v_w$; (turbulence Tu);
- air supply system: pressure difference $\Delta p_e$;
- relevant fluid properties: $\rho_w$; g; $\mu_w$; $\sigma_{wa}$.

The fluid properties of air can usually be neglected. For a given geometry, this set of variables also describes the downstream flow conditions completely.

For the dependence of the specific rate of entrained air, for instance, we can now write

$$q_{ae} = f(\text{geometry}; l_w; v_w; (Tu); \Delta p_e; \rho_w; g; \mu_w; \sigma_{wa}) \qquad (1.1)$$

where the left hand side could be replaced by any other dependent variable of interest. A classical dimensional analysis leads to

$$\frac{q_{ae}}{v_w l_w} = f\left(\text{geom. ratios}; (Tu); \frac{\Delta p_e}{\rho_w v_w^2/2}; \frac{v_w}{\sqrt{g l_w}}; \frac{v_w \cdot l_w}{\mu_w/\rho_w}; \frac{v_w}{\sqrt{\sigma_{wa}/\rho_w l_w}}\right) \qquad 1.2)$$

or

$$\beta_e = \frac{q_{ae}}{q_w} = f(\text{geom. ratios}; (Tu); c_{pe}; Fr; Re; We) \qquad (1.3)$$

and alternatively by the rules of dimensional analysis (Kobus 1973) to

$$\beta_e = f(\text{geom. ratios};\ Tu\ ;c_{pe};Fr;Re;Z \equiv \frac{g \cdot \mu_w^4}{\rho_w \cdot \sigma_{wa}^3}) \qquad (1.4)$$

and corresponding relationships for all other dependent variables, including the turbulent flow characteristics like turbulence intensity or turbulent energy spectrum. The relationship (1.4) represents the complete similarity requirements for local aeration processes.

As an alternative to the Weber number, which describes the relative importance of inertial forces and surface tension, the liquid parameter Z can be used. This parameter has the obvious advantage that it contains neither the reference length nor the reference velocity. It is a function of the liquid properties alone and thus independent of the boundary scale and the flow velocity. For pure water, the value of the liquid parameter is ($Z \approx 10^{-11}$); it will remain constant as long as temperature and water quality remain unchanged. In evaluating small scale model studies, this set of parameters has the advantage that "scale effects" in Froude models, for an invariant Z, are now concentrated in the effects of the Reynolds number. Otherwise, equations (1.3) and (1.4) are completely equivalent.

## 1.6 General controlling conditions

The process of air entrainment is subject to several limiting conditions. We can distinguish an inception limit, entrainment limit, air supply limit and transport limit. Each one of these may be the controlling factor: therefore, in comparing flow configurations of different geometry or size, attention has to be paid to all of these limits.

(1) Inception limit

For a given flow configuration, the flow conditions must be such as to generate a sufficiently large disturbance for air entrainment to occur. The inception limit depends strongly upon the fluid properties and characterizes the condition that inertial reactions become large enough to overcome the resisting forces due to viscosity and surface tension. In general, a certain minimum velocity has to be exceeded, and the initiation of air entrainment is greatly enhanced by turbulent fluctuations of the approach flow.

(2) Entrainment limit

The conditions of the approach flow govern the entrainment limit. These conditions are quantified by the Froude number Fr. depending upon the boundary geometry, a critical value of Fr must be exceeded to ensure the formation of a surface disturbance or discontinuity at which air entrainment can occur (e.g. $Fr > 1$ for the hydraulic jump). For higher Froude numbers, the approach flow provides the driving mechanism for the air entrainment. In most cases, the air entrainment process is not directly affected by the local boundary scale.

(3) Air supply limit

In flow configurations such as spillway aerators (Fig. 1.9 and Fig. 1.10), air is entrained from a limited enclosed air space, which is connected to the atmosphere by an air duct. In these cases, the supply of air to the point of entrainment into the water requires an air flow through a duct system. This flow necessarily results in a pressure difference between the ends of the air duct. The subatmospheric pressure at the location of air entrainment depends upon the air entrainment rate and the air

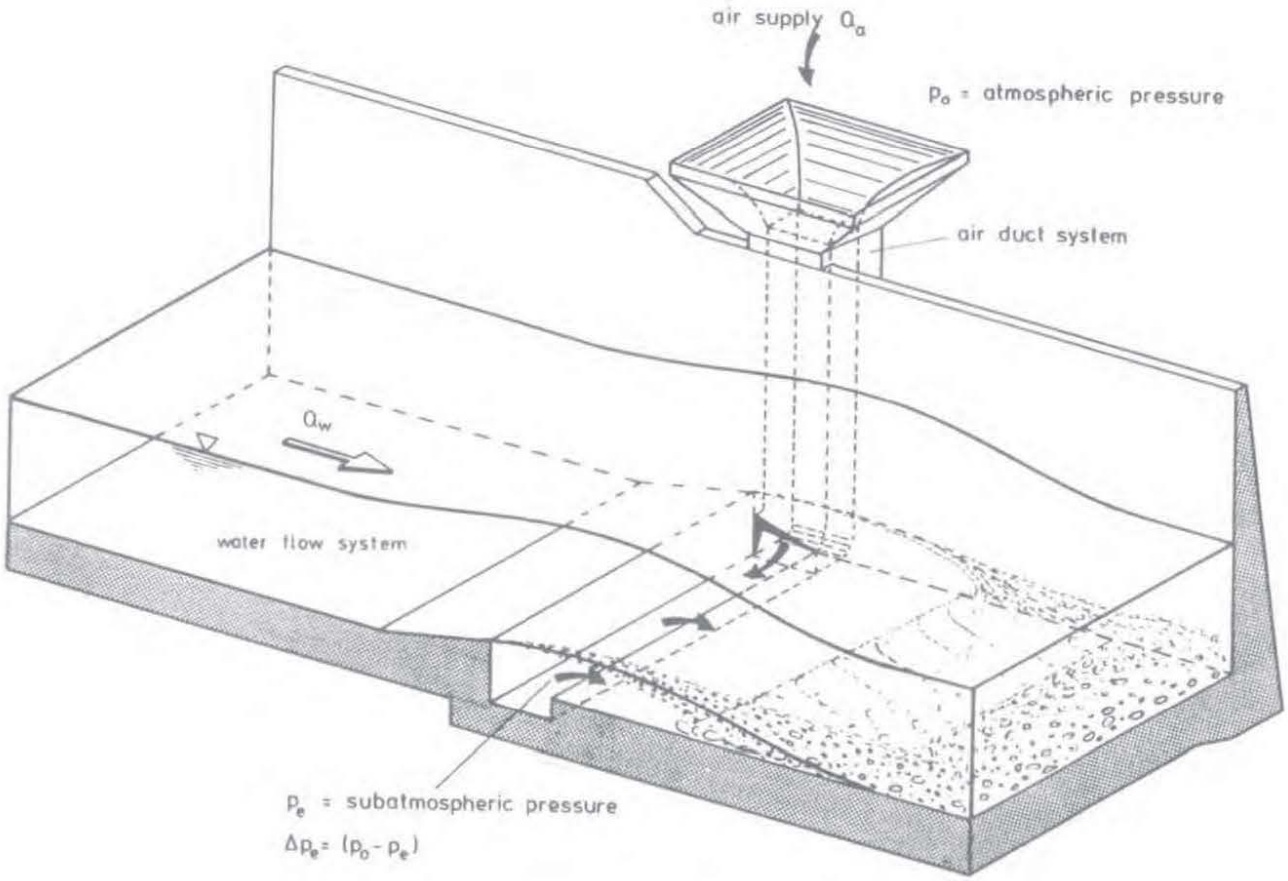


Fig. 1.9: Air supply system of an aerator device

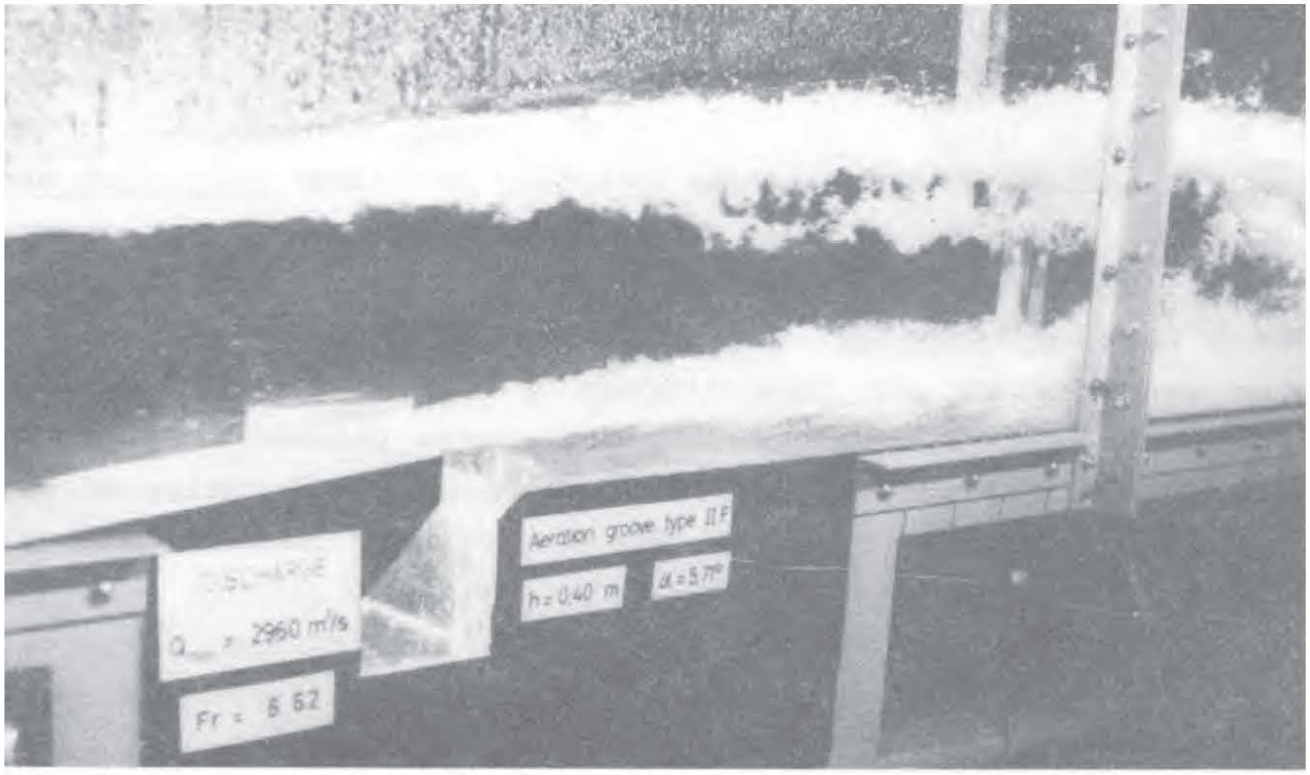


Fig. 1.10: Air entrainment in an aerator device (sectional model)

duct resistance. As is sketched in Fig. 1.11, the pressure difference is a maximum when the air duct is closed and decreases to zero for unlimited air supply. Depending upon the head loss characteristics of the air duct system, there results an operating point characterizing the resulting air supply rate and the corresponding pressure difference. In this case, the air supply system is limiting the air entrainment.

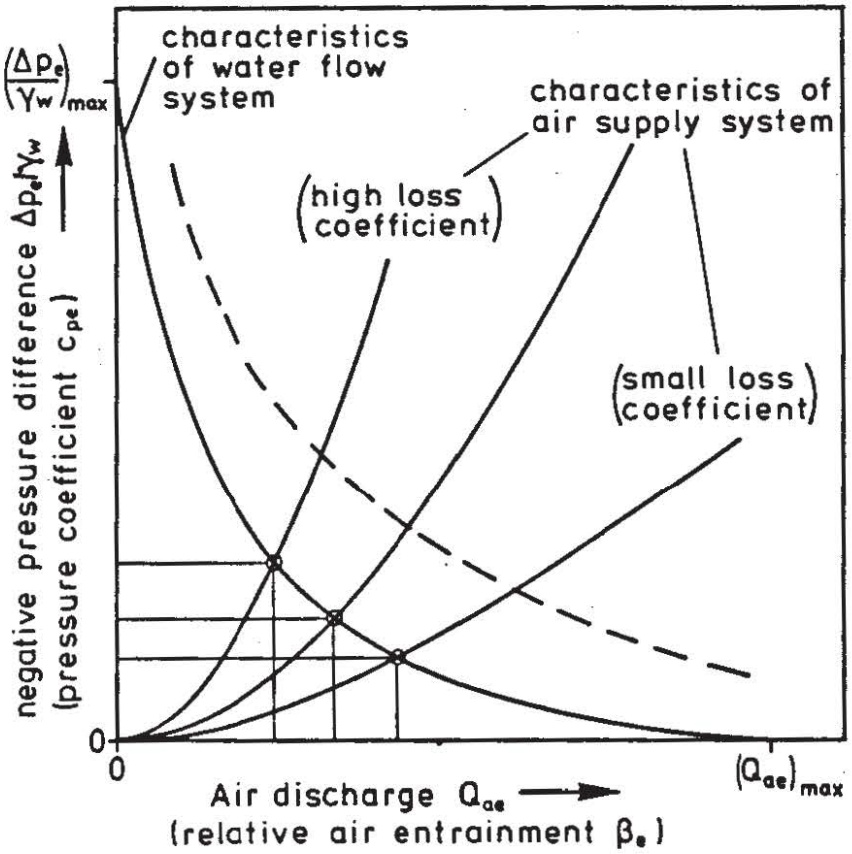


Fig. 1.11: Air supply control

(4) Transport limit

The transport capacity of the flow is governed by the downstream flow conditions. It depends upon the flow velocity and turbulence as determined by the wall shear stresses (Wood, 1983). An upper limit for air transport is given by the maximum possible air bubble concentration in the flow (Brauer, 1971).

## 1.7 Air bubble formation and transport

### 1.7.1 Bubble formation

The process of air entrainment involves the entrapment of an air volume at the surface, the breakup of the entrapped air volume into an array of bubbles, and the subsequent transport by the flow, during which the bubble size distribution may change due to coalescence or breakup of individual bubbles. At the entrainment location, air is entrapped in the low pressure core of vortices and is transported into the water until the cores decay and the pressure differences become small and the air bubbles are released. Whereas the entrapment and initial breakup are governed by inertial and gravitational forces and hence Froude-number dependent, the bubble transport is governed by the turbulence characteristics and hence the Reynolds number of the flow.

The entrapment and bubble formation process at local surfaces discontinuities is related to the turbulent shear stress generated between approach flow and receiving water body. Here, the scale and intensity of the turbulent fluctuations in the approach flow play a predominant role. Ervine, 1985, argues that the bubble diameter generated is a function of the turbulence characteristics at the entrainment location, with peak turbulence levels entraining small air pockets and median turbulence levels entraining mean size air pockets, etc. He therefore concludes from the fact that the shear layer turbulence shows a Gaussian distribution that the resulting bubble diameters should also follow a Gaussian distribution curve.

A frequently investigated process of bubble formation is the breakup of a continuous air jet discharging from a nozzle into a water body. Analytical considerations on instability and breakup of air pockets by Rayleigh have been verified experimentally (Kobus, 1973). At injection of a continuous air jet through a nozzle into an otherwise stagnant water body, the air jet

immediately breaks up into an array of bubbles which range in diameter from almost zero up to a maximum value, which depends upon the air discharge $Q_o$ and gravitational acceleration g (Kobus, 1973):

$$d_{b_{max}} = (1.295 \text{ to } 1.487)\,(Q_o^2/g)^{1/5} \qquad (1.5)$$

In free-surface aeration, there will also result a mixture of bubbles up to a certain maximum size; no information is available, however, about the magnitudes involved.

Numerous visual observations and some measurements of bubble sizes in turbulent flows (excluding here high speed flows with $v_w \gg v_b$) have shown that the majority of the larger bubbles are in the range of 1 to 10 mm, and that the mean bubble diameter decreases with increasing turbulence. Some examples of measured bubble size distributions in air bubble screens are shown in Fig. 1.12. From these observations one may suspect that turbulent flows of air-water mixtures should finally reach a state of equilibrium with a certain turbulence structure and a corresponding bubble size distribution.

In high-speed flows ($v_w >> v_b$), it is surmised that the resulting bubble sizes are smaller than the range given above. The higher the resulting shear rates, the smaller will be the air bubbles. Observation in spillways indicates that bubble sizes are small near the bed and increase with increasing distance from the bed.

Air bubbles of finite size always exhibit a slip velocity $v_b$ relative to the surrounding water. To a reasonable degree of approximation, this slip velocity corresponds to the rising velocity of a single bubble in an infinite fluid otherwise at rest. The flow field can therefore be considered as a combination of the water flow field with the bubble slip velocity superimposed. (In high-speed flows, this effect is small).

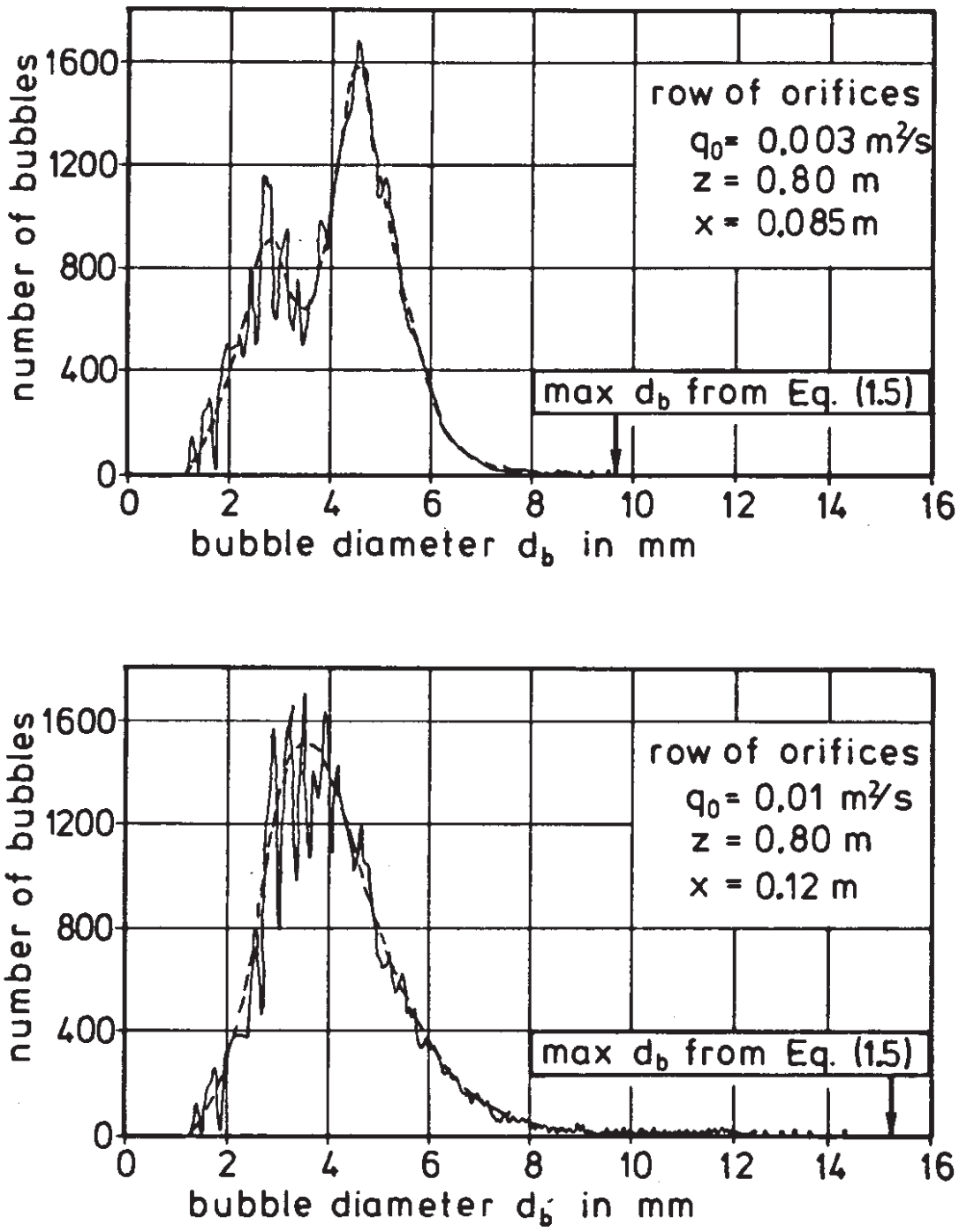


Fig. 1.12: Examples of bubble size distributions in turbulent flow: Measurements of Barczewski 1979 in a plane bubble plume at an elevation z and lateral distance x from plume axis

1.7.2 Bubble slip velocity: single bubble in stagnant water

The behaviour of a single gas bubble in a liquid has been studied extensively. A dimensional analysis for the bubble rise velocity $v_b$ of a bubble of diameter $d_b$ yields

$$c_d \equiv \frac{4g \cdot d_b}{3 v_b^2} = f\left[Re \equiv \frac{v_b d_b}{\mu_w/\rho_w} ; Z \equiv \frac{g \cdot \mu_w^4}{\rho_w \sigma_{wa}^3}\right] \qquad (1.6)$$

with

| | | |
|---|---|---|
| $c_d$ | (-) | drag coefficient |
| $g$ | (m/s²) | gravitational acceleration |
| $d_b$ | (m) | equivalent bubble diameter (sphere of equal volume) |
| $v_b$ | (m/s) | bubble rise velocity |
| $\mu_w$ | (kg/m s) | dynamic viscosity of the liquid |
| $\rho_w$ | (kg/m³) | density of the liquid |
| $\sigma_{wa}$ | (N/m) | surface tension at the liquid-gas interface |

The quantitative relation between these parameters is given in Fig 1.13. This diagram shows a nearly universal relation between $c_d$ and Re, in which the influence of the liquid paramter Z is pronounced merely in the region of Reynolds numbers between $10^2$ and $10^3$. This indicates that for Reynolds numbers smaller than $10^2$ (small bubbles) and larger than $10^3$ (large bubbles) the $c_d$-versus-Re relation can be considered as universal and valid for any kind of gas or liquid, whereas in the intermediate region ($10^2 < Re < 10^3$), the liquid parameter (and hence the water quality) plays an important role.

For the case of very small spherical bubbles, an exact expression has been obtained for this relationship. Surface tension is the predominant force determining the shape of very small bubbles. Therefore, small bubbles tend to be almost perfect spheres. The motion of these bubbles through a fluid can be described by a balance betweeen the buoyant forces and the viscous forces. Since the bubble behaves like a rigid sphere, Stokes solution applies:

$$c_d = \frac{24}{Re} \qquad \text{for small Re} \qquad (1.7)$$

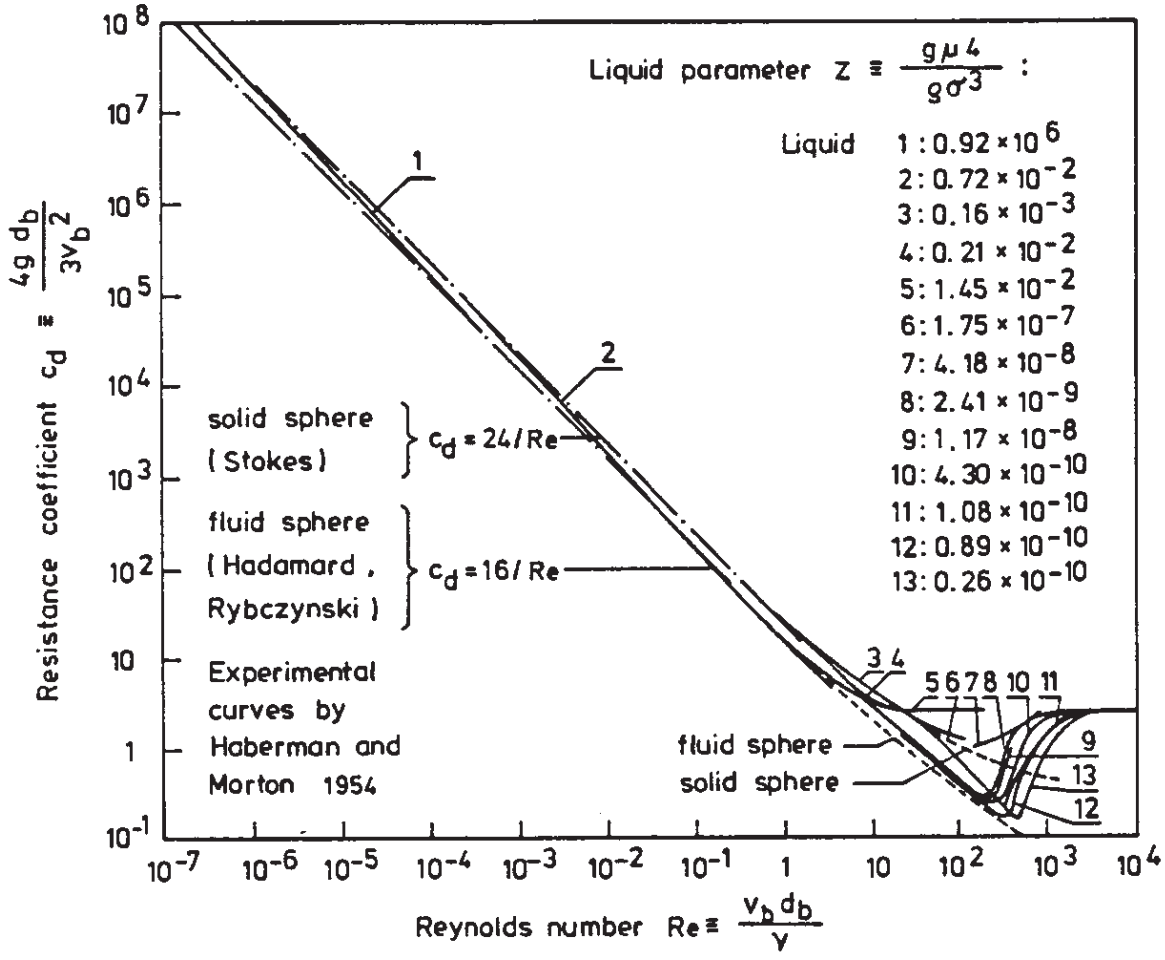


Fig. 1.13: General resistance diagram for gas bubbles in liquids

The region of validity of this relation depends upon the magnitude of Z (see Fig. 1.13). In terms of the bubble rise velocity $v_b$, this can be expressed as

$$v_b = \frac{1}{18}\,\frac{d_b^2 g}{\nu_w}\left(1 - \frac{\varrho_a}{\varrho_w}\right) \qquad \text{for small Re} \qquad (1.8)$$

For slightly larger bubbles, a spherical shape and straight rising path is maintained, but an internal gas circulation is set up which results in a relationship of the form

$$c_d = \frac{16}{Re} \qquad (\text{for } Re < 10^2) \qquad (1.9)$$

or in terms of bubble rise velocity

$$v_b = \frac{1}{12}\,\frac{d_b^2 g}{\nu_w}\left(1 - \frac{\varrho_a}{\varrho_w}\right) \qquad (\text{for } Re < 10^2) \qquad (1.10)$$

It is to be noted that the transition to this range depends strongly upon the liquid parameter Z. For water, which has an extremely low value of ($Z \approx 10^{-11}$), no experimental evidence for this flow regime is known.

As the bubbles become larger, inertial effects become important and the bubble shape is changing in accordance with the pressure distribution over the surface. With increasing size, the bubble shape changes to an oblate spheroid, and the bubble rises along an irregular or spiral trajectory. For this region, numerous empirical formulas describing the bubble rise velocity have been proposed. However, all of these relations are valid only for a limited range and strongly influenced by the liquid parameter Z.

Very large bubbles attain a spherical cap shape with an included angle of the spherical front surface of about 100 degrees and a relatively unstable flat base. These large bubbles follow again a straight rising path. The bubble rising velocity in this range is characterized, according to Haberman and Morton (1953), by

$$c_d = 2.6 = \text{const} \qquad \text{for } (Re > 2 \cdot 10^3) \qquad (1.11)$$

or else

$$v_b = 0.716 \sqrt{g \cdot d_b} \qquad \text{for } (Re > 2 \cdot 10^3) \qquad (1.12)$$

For the specific case of air bubbles in natural water bodies, this results in a relationship between terminal rising velocity and equivalent bubble diameter (diameter of sphere of equal volume) as given in Fig. 1.14. This relationship has been determined experimentally by Haberman and Morton (1953). It exhibits the same parameter dependence as Fig. 1.13. For the fluid properties of air and water at 10°C of

$$\nu_w \approx 1.3 \times 10^{-6} \ \text{m}^2/\text{s}$$
$$\rho_w \approx 1000 \ \text{kg/m}^3$$
$$\rho_a \approx 1.25 \ \text{kg/m}^3$$

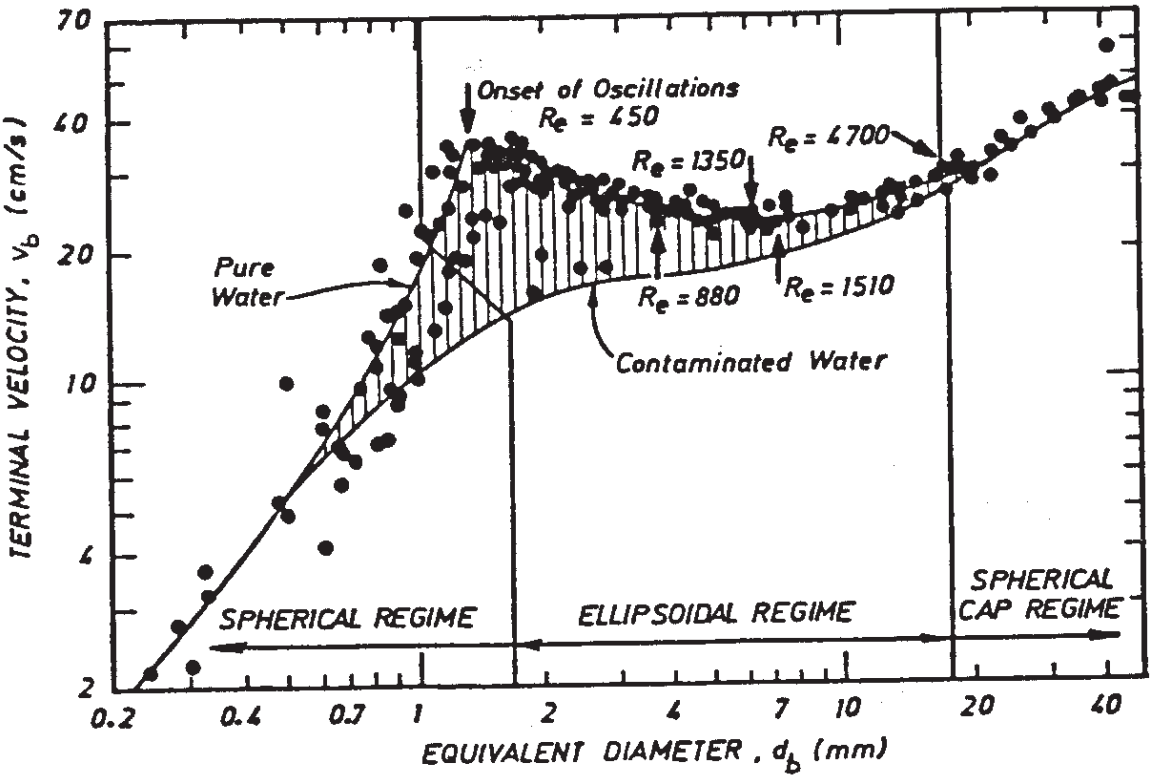


Fig. 1.14: Terminal bubble rise velocity $v_b$ of a single air bubble in an extended waterbody otherwise at rest (Haberman and Morton, 1954)

one obtains the following dimensional relationship for small bubbles, corresponding to Eq.(1.8) for (Re < 1):

$$v_b(m/s) = 0.362\ d_b^2\ (mm) \qquad \text{for } (d_b < 0.2 \text{ mm}) \qquad (1.13)$$

For intermediate bubble diameters between 0.2 and 20 mm, the air bubble rising velocity can be taken from Fig. 1.14. In this range, variations due to water quality (i.e. variations of the parameter Z) are evident, with velocities anywhere between 0.1 and 0.4 m/s. Ellipsoidal shapes and spiral motions are observed for bubble diameters exceeding 1 to 2 mm. In pure water, a pronounced maximum velocity is observed for bubbles slightly larger than 1 mm in diameter, which decreases again for larger bubble sizes. In contrast, contaminated water does not exhibit this peak and gives considerably different values.

For very large bubbles of spherical cap shape, one obtains a unique relationship corresponding to equation (1.12) as

$$v_b(m/s) = 0.071\ d_b^{1/2}(mm) \qquad \text{for } (d_b > 10\ mm) \qquad (1.14)$$

1.7.3 Motion of a bubble cloud in stagnant and moving water

If a multitude of air bubbles is released in a laterally unrestricted stagnant water body, the ensemble will rise to the surface with a considerably larger mean velocity than a single bubble. This is due to the fact that the bubble swarm induces an upward water flow which adds to the individual bubble slip velocity. On the other hand, if the water has a horizontal velocity component, this effect is counteracted to some degree by the fact that the bubbles are displaced laterally along their path and hence the induced vertical water flow is less pronounced. An air bubble plume is shown in Fig. 1.15.

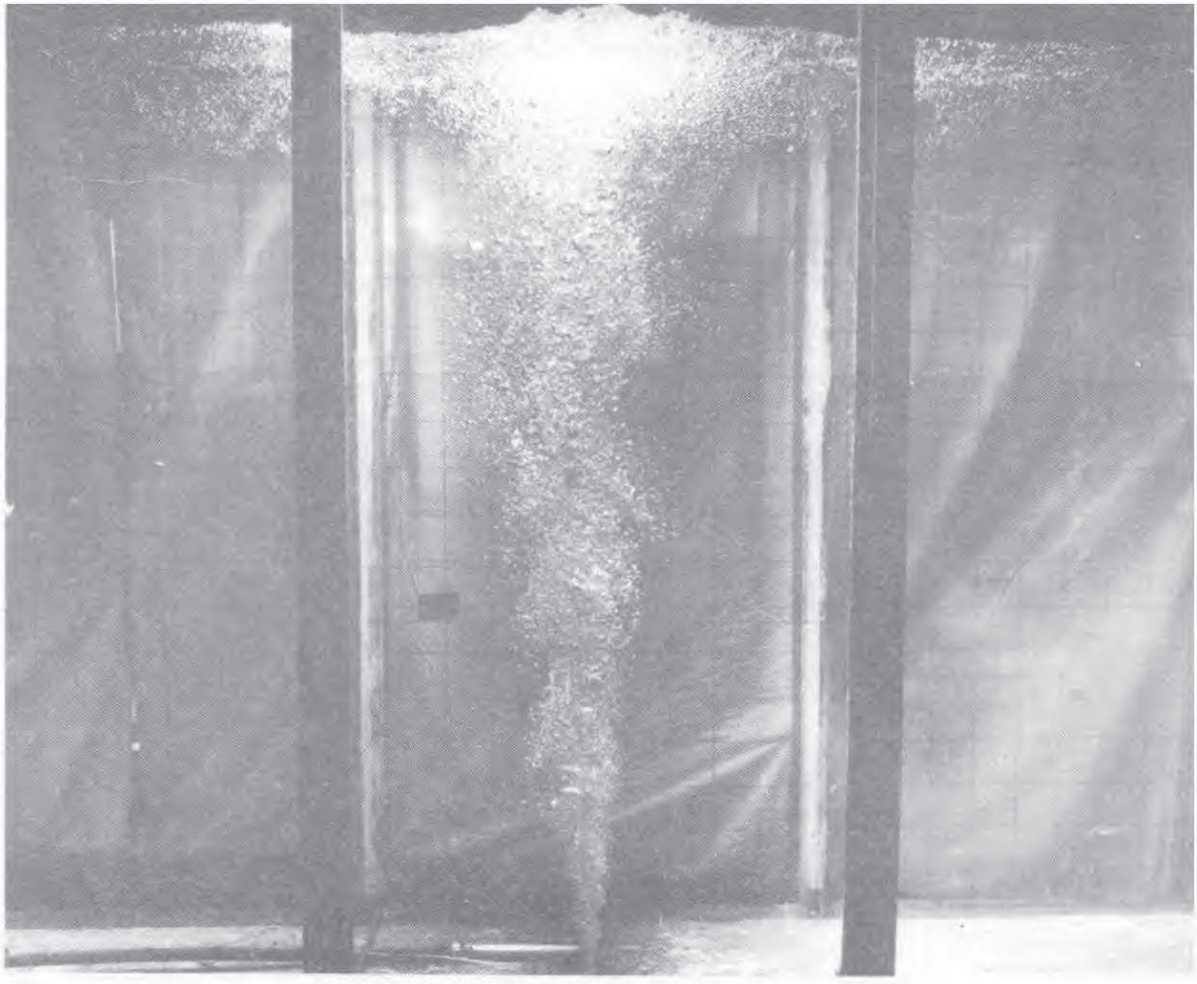

Fig. 1.15: Air bubble plume

As an orientation for the magnitude of the effects involved, Figs. 1.16 and 1.17 show some experimental data for average rising speeds of bubble clouds above single orifices and above rows of orifices, respectively. These data demonstrate two points:

(1) The air bubbles induce a substantial vertical water velocity, leading to effective rising velocities which are two to three times higher than for a single bubble.

(2) Even moderate cross flow velocities dramatically counteract this bubble-induced flow and quickly reduce bubble-rise velocities again to the order of magnitude of the slip velocity of single bubbles.

It is to be noted that the air bubble plumes described above rise in a laterally unconfined flow. In the presence of lateral confining boundaries, the mean rising velocity will be hindered by the fact that the displaced water will induce a downward counterflow for continuity reasons - much in the same way as the side - wall effect of a narrow tube on the settling of a single particle. In flow configurations where bubbles occur in the entire flow region (as on spillways, e.g.), the mean bubble rising velocity must by continuity be the hindered velocity.

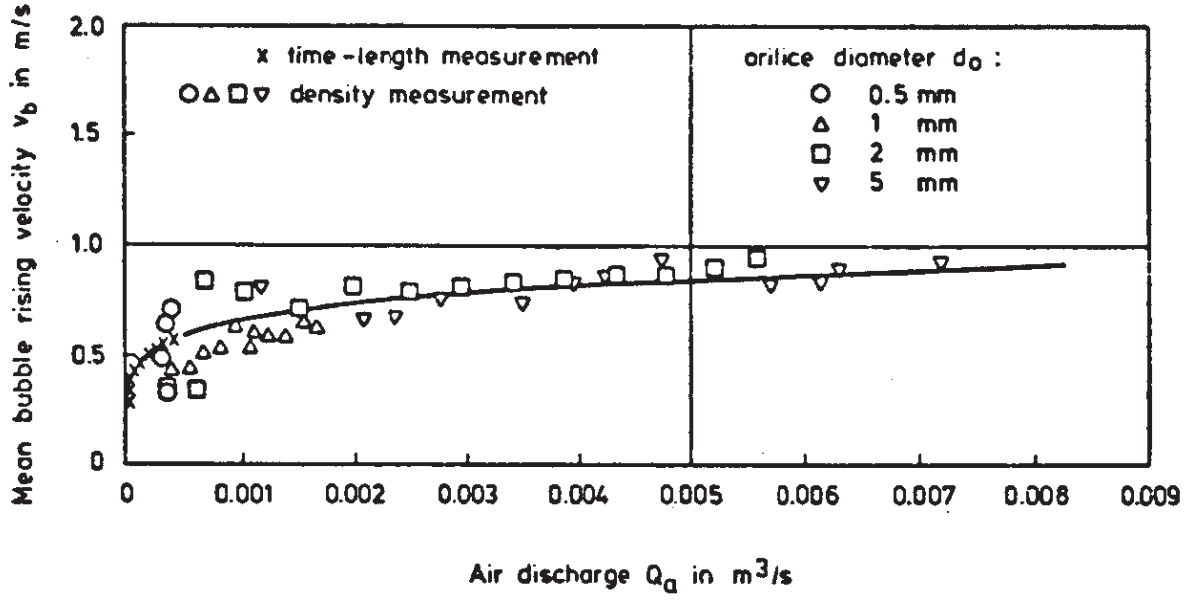


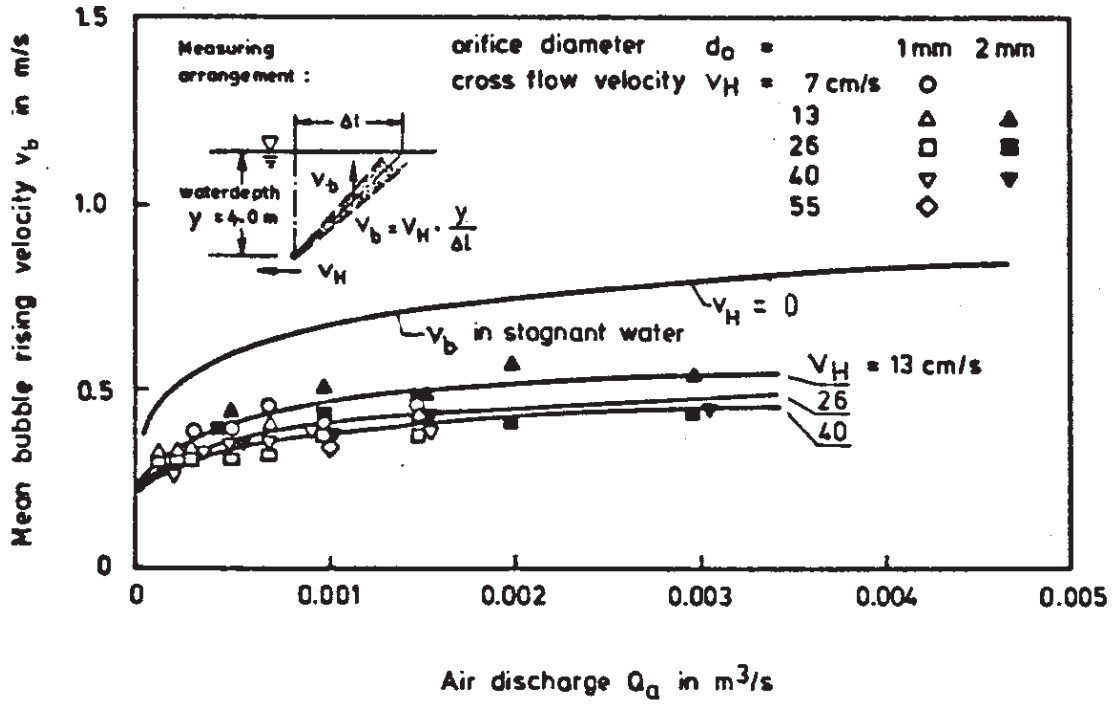


Fig. 1.16: Mean rising velocity of bubble ensembles in a bubble plume above an orifice

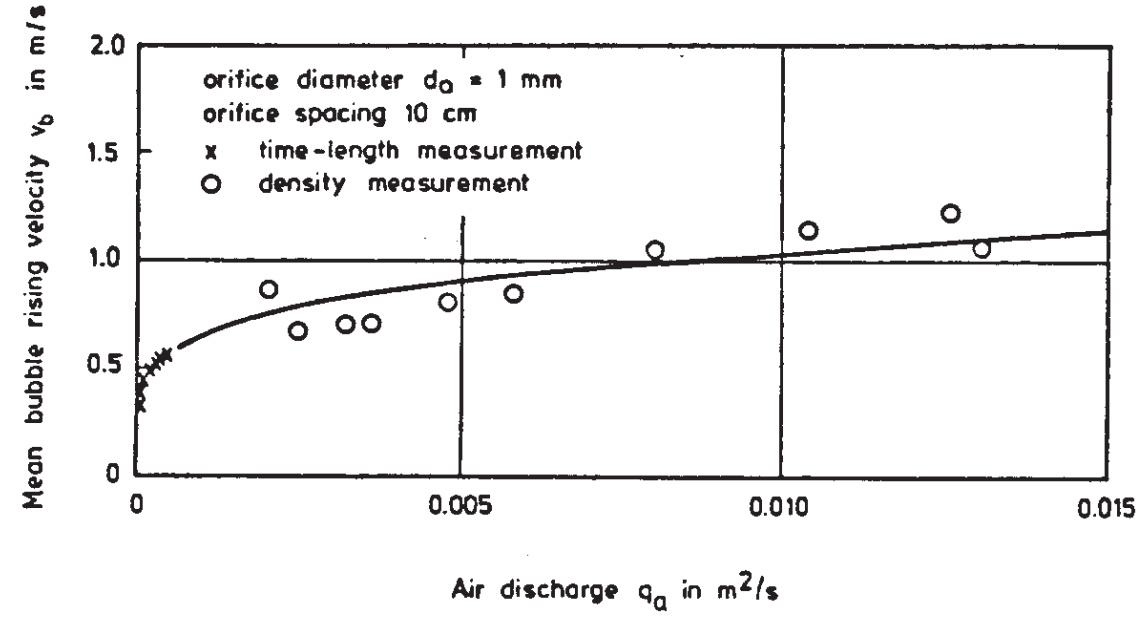


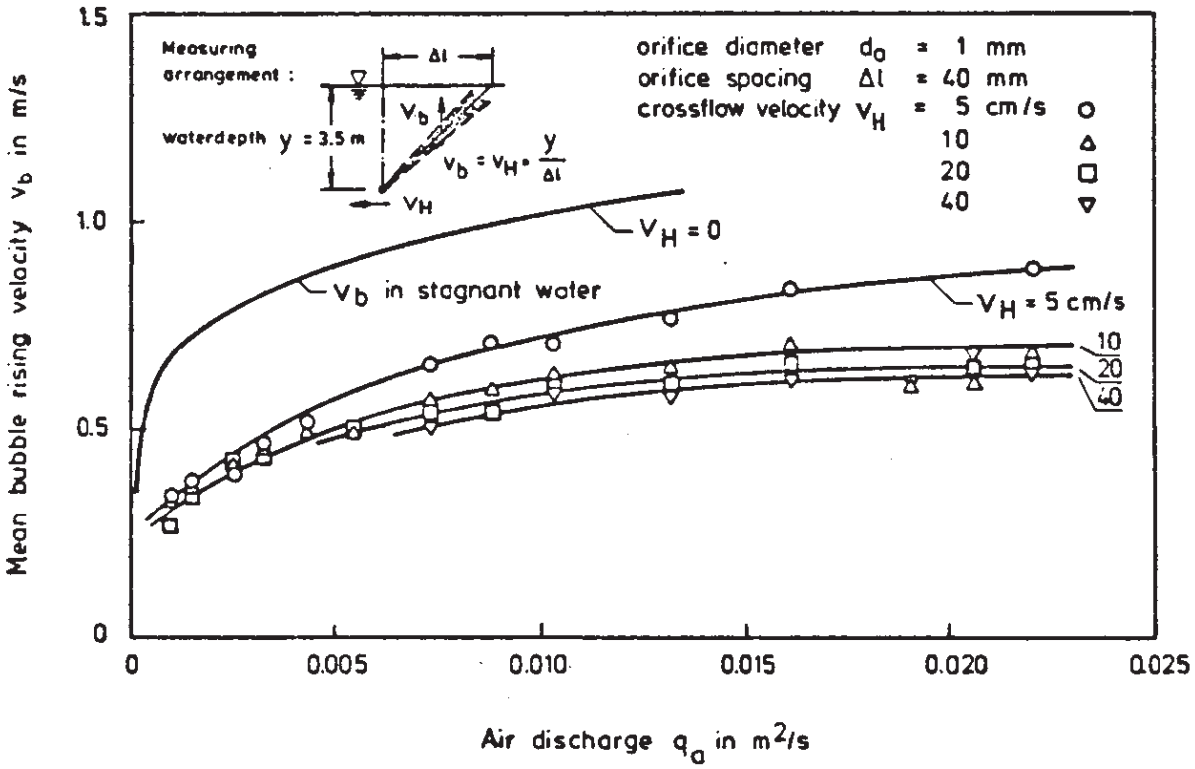


Fig. 1.17: Mean rising velocity of bubble ensembles in a plane bubble plume (row of orifices)

1.7.4 Effect of turbulence upon air bubbles

Air bubbles are greatly affected by flow turbulence. This is primarily turbulence in the carrying water flow generated either by wall shear (bottom friction) or by free shear layers (jet impingement, surface roller, separation zones). However, the presence of the air bubbles also contributes to the turbulent fluctuations (bubble-induced turbulence), and in stagnant water bodies this is the only source of turbulence.

Turbulent fluctuations can be responsible for

- breakup of large air bubbles due to shear action;
- coalescence of small bubbles in the core of vortices in the flow, since the air follows pressure gradients in the flow much more rapidly than water because of its much smaller inertia.

In open channel flows, the water flow direction is primarily parallel to the channel bottom, and the wall-friction-induced turbulent fluctuations (RMS) $v_t = \sqrt{\overline{v'^2}}$ increase to a first approximation linearly with the mean water flow velocity $v_w$. By comparing the water velocity $v_w$ to the bubble velocity $v_b$, which is of the order of magnitude of 30 cm/s, one can hence distinguish:

- Nearly stagnant water bodies ($v_w << v_b$), such as lakes or reservoirs, with essentially bubble-induced turbulence,
- slowly flowing water ($v_w \approx v_b$) with pronounced air-water interaction, and
- high-speed flows ($v_w \gg v_b$) with pronounced effects of the water flow turbulence upon the air bubbles. For this range, Thomas et al. (1983) studied the entrapment and transport of small bubbles by discrete vortices in a shear layer. Using both a numerical and a physical model, they could show that small air bubbles rising in water are trapped and transported by the vortices.

## 1.8 Bubble-induced water flow

In stagnant ($v_w << v_b$) or in slowly flowing water ($v_w \approx v_b$), the effects of the bubbles on the flow field may be quite pronounced. The entrained air bubbles exert a buoyancy force on the surrounding water, which gives rise to a bubble-induced water flow. This can best be illustrated by considering a bubble plume generated by injection of compressed air at the bottom of a stagnant water body. In this case, the resulting mean and turbulent flow field is entirely due to the buoyancy of the induced air discharge and to the dynamics of the bubble swarm (purely bubble-induced turbulence).

The flow field of air and water in bubble plumes (Kobus 1973) is characterized by the fact that the vertical momentum flux of the induced water flow increases with upward distance from the air source due to the action of the bubble buoyancy. The buoyancy force input $F_B$ per unit time is given by the amount of entrained air:

$$F_B = (\rho_w - \rho_a) \cdot g \cdot Q_a \approx \rho_w \cdot g \cdot Q_a \qquad (1.15)$$

and with this the vertical momentum flux $M_{w,z}$ can be expressed as

$$\frac{dM_{w,z}}{dz} = F_B - F(v_b) \qquad (1.16)$$

with $F(v_b)$ representing the resistance force to the slip velocity $v_b$. If the bubbles would be infinitely small (i.e. zero slip velocity and hence also $F(v_b) = 0$), then the flow field should correspond to the classical buoyant plume. However, bubbles of finite size do exhibit a slip velocity $v_b$ relative to the surrounding water, which results in a correspondingly smaller increase of the water momentum flux. The acting buoyancy force $F_B$ is partly used up for moving the air bubbles through the liquid (resistance force $F(v_b)$ to slip velocity) and only the remaining part acts to increase the water momentum flux $M_{w,z}$.

This illustrates the importance of the bubble sizes for the concentration and velocity distribution: the larger the bubbles, the higher the slip velocity $v_b$ and the less pronounced the induced water velocity.

In contrast, the horizontal momentum flux of the water flow remains essentially unaffected by the presence of the air bubbles. The negligible density of the air bubbles allows them to be transported laterally by the water flow without considerable slip velocities. The only noticeable change for the horizontal flow components will therefore be, in high air concentrations, an effect upon the local mixture density to be considered in the momentum equation.

It follows from these considerations that the most pronounced effects of air bubbles upon the water flow are to be expected in predominantly vertical flow configurations, such as plunging jet or drop shaft arrangements, but play a lesser role in predominantly horizontal flows. As an illustrative example for the drastic effects that entrained air can have on the water flow field, two flow situations in a drop structure are shown in Fig. 1.18, which are described in detail by Kobus and Westrich (1983).

In high-speed flows (e.g. on spillways) with water velocities of one or two orders of magnitude above the bubble rising velocities, the dynamic effects of the air bubbles on the flow can be neglected and the bubbles can be considered to behave almost like an inert tracer or else like fine suspended sediment particles.

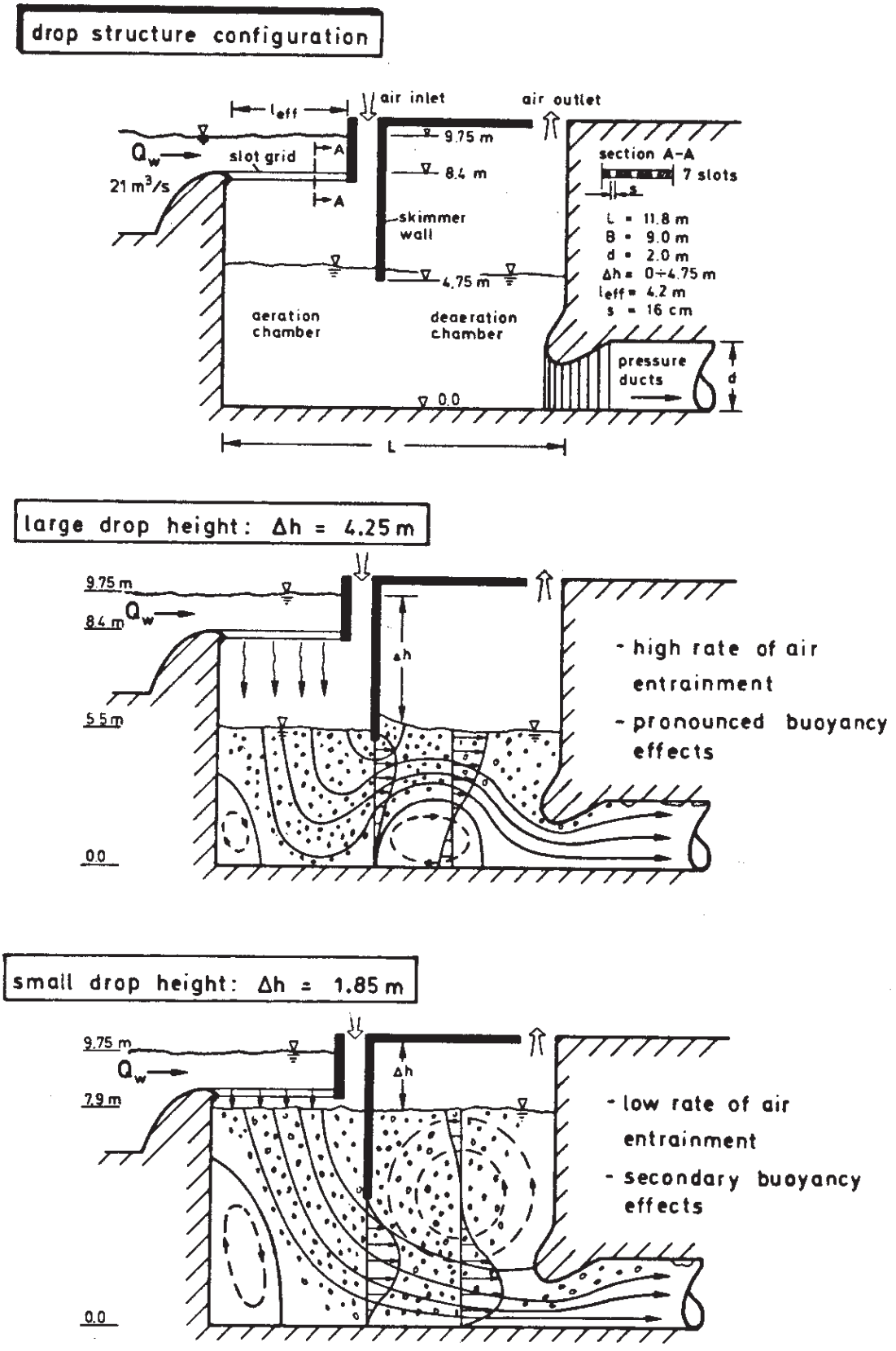


Fig. 1.18: Effects of air buoyancy on the flow field in a drop structure (Kobus and Westrich, 1983)

# 2. LOCAL SURFACE AERATION AT HYDRAULIC STRUCTURES

## 2.1 Introduction

In open channel flows, local surface aeration processes occur mainly at weirs and drop structures and in hydraulic jump configurations. Air entrainment in the wake of bluff bodies is observed only in high speed flows.

In water pollution abatement, the natural gas exchange at the free surface is sometimes not sufficient to balance the oxygen consumption due to pollutants. In such cases, local aeration in order to increase the oxygen transfer into the water body is needed. In this context, hydraulic structures leading to local surface aeration provide the increased oxygen transfer by way of the entrained air bubbles. Thus the air-entrainment and oxygen-transfer characteristics have become an important design criterion for many hydraulic structures. Contrary to the structural design considerations, which would seek to avoid air entrainment, water quality considerations are geared towards increasing the air entrainment rates.

Local surface aeration processes are highly complex phenomena which depend very sensitively upon many parameters. The importance of the boundary geometry and of the absolute scales of geometry and flow rates must be emphasized. Therefore, no generally applicable design criteria can be formulated at this time. Each of the flow configuration described in chapter 1 and each of the various limitations of the entraining process has to be studied in detail.

The following chapter is an attempt to summarize the available information about local air entrainment and oxygen transfer in such a way that it may serve as an orientation for preliminary design considerations. Limited results can be presented for a small number of flow geometries. These results can only be used

for similar geometries, and it is necessary to check that the flow configurations are really comparable. Application of these results to other flow configurations could lead to greatly erroneous estimates.

It must be furthermore emphasized that the majority of results presented here stem from laboratory investigations at small scales. These data can only be safely applied within the range of scales and discharges in which they have been obtained. This range is therefore quoted for all empirical relationships. Extrapolations beyond this range must take into account the possible scale effects involved (Kobus, 1984).

Because of the absence of generally applicable standard design criteria, the following chapter can only identify the major effects involved in local aeration, give the available data for standard geometries, and provide a discussion of the similarity considerations for hydraulic model studies.

## 2.2 Parameters governing local aeration

In most cases of local aeration, air entrainment takes place at a discontinuity of the free surface at which substantial velocity differences are encountered. In a hydraulic jump, for instance, the air is entrained exclusively at the toe of the surface roller. In impinging jets penetrating into a stagnant water body, air is entrained along the circumference of the jet intersecting the free water surface. The essential local parameters governing the entrainment process are

- the velocity $v_e$ (or velocity difference) at the line of air entrainment;
- the length (width) of the intersection line, at which air is entrained;
- the character (smoothness) of the water surface at the line of air entrainment. This is characterized by the intensity and

scale of the turbulence of the approach flow and possibly also the air content of the approach flow;
- density $\rho_w$ and gravity g.

If this is common to all configurations, it may be used in order to distinguish
- the "outer problem": how do these local characteristics depend upon the system parameters of the structure?
- the "inner problem": how does the air entrainment depend upon the local characteristics?

In looking at the "inner problem", a crucial point is the observation that there is no physically meaningful geometric boundary reference length involved in the air entrainment process. It follows from the description of the entrainment process given below that the significant length terms are the turbulent eddy size and the air pocket size, which are both dependent variables governed by the fluid properties and the flow and not prescribed by the boundary configuration. The water depth or jet width (as geometric boundary length) is in most cases irrelevant and only of importance at small values (order of magnitude 0,01 m).

The process of air entrainment can be visualized as air pockets being trapped between roller or water surface and inflow, which are then carried away in the downstream direction. The size and frequency of formation of such pockets can reasonably be expected to depend upon the differential velocity between the receiving water volume and the inflow, or - since the former is zero in the mean - upon the velocity of the inflow alone. This velocity governs the turbulent shear stress generated in the shear layer at the entrainment location. Obviously, the boundary scale - for instance, the water depth or jet width - will in most cases have no influence upon the entrainment process unless it becomes small enough to be of the order of the enclosed air pockets. This fact can be used to deduce some information about the inception and entrainment limits.

In Chapter 1, the distinction was made between plunging jet-type configurations and surface-roller type configurations, the former being predominantly vertical and the latter predominantly horizontal. As a further point in contrast to jet flows, the surface roller in hydraulic jumps is governed by the downstream water depth, which in turn results from the approach flow Froude number, which includes the upstream water depth (see Fig. 1.6).

## 2.3 Inception limit

The inception of air entrainment is governed by the condition that the free surface is penetrated and interrupted by the impinging flow. Air entrainment will commence when inertial and gravity forces override the resisting forces due to viscosity and surface tension. Therefore, the "critical" velocity $v_c$ for onset of aeration will depend, for given approach flow conditions, on the following fluid properties:

$$f(v_c; \rho_w; g; \mu_w; \sigma_{wa}) = 0 \qquad (2.1)$$

These can be grouped into two dimensionless parameters:

$$f\left(\frac{v_c^3}{g\mu_w/\rho_w}\,;\ \frac{g\mu_w^4}{\rho_w\,\sigma_{wa}^3}\right) = f\left(\frac{v_c^3}{g\nu_w}\,;\ Z\right) = 0 \qquad (2.2)$$

This means that the nondimensional critical velocity will depend upon the magnitude of the liquid parameter Z, and if Z is kept constant (constant water quality and temperature), the inception limit is characterized by

$$\frac{v_c^3}{g\mu_w/\rho_w} = \text{const} \approx (0.5 \text{ to } 1) \times 10^5 \qquad (2.3)$$

The order of magnitude given is a rough estimate taken from experimental evidence for plunging water jets, which indicates that air entrainment commences at velocities of 0.8 to 1 m/s.

Equation (2.3) indicates that the inception limit neither corresponds to a constant Reynolds number nor to a constant Froude number.

When the approach flow is turbulent, two additional parameters must be introduced, which characterize the intensity and scale of the turbulent fluctuations. If $v_t$ denotes the RMS of the velocity fluctuations and $l_t$ is a turbulence length scale, then one arrives by dimensional analysis at

$$\frac{v_c^3}{g\mu_w/\rho_w} = f\left[\frac{v_t}{\mu_w^3 g/\sigma_{aw}^2\rho_w}\ ;\ \frac{l_t}{\sigma_{aw}^2/\mu_w^2 g}\ ;(Z)\right] \qquad (2.4)$$

where $\sigma_{aw}^2 / \mu_w^2 g$ is a length scale based on the fluid properties and gravity.

A physical concept of the plunge point inception has been outlined by Thomas, 1982. It relates air entrainment to the fact that the plunge pool water is unable to follow undulations of the jet surface and hence small air pockets are formed. Surface undulations in turn are produced by the turbulence in the jet as described by Eq. (2.4).

The experimental results for plunging jets obtained by Ervine et al. (1980) indicate that the critical velocity depends strongly upon the turbulent velocity fluctuations $v_t$, whereas the jet diameter and hence the scale $l_t$ of the large eddies in the approach flow is insignificant. It can therefore be concluded that for given fluid properties (Z = const) the critical velocity $v_c$ will depend upon the relative turbulence $(v_t/v_w)$ or $(v_t/v_c)$. Ervine's results for jet diameters of 6, 9, 14 and 25 mm are plotted in Fig. 2.1. It can be seen that for larger turbulence intensities $v_c$ is almost constant in the range of 0.8 to 1 m/s. Ervine suggests further that for an impinging rectangular water jet the critical velocity is also in the same range. Observations by Casteleyn and Kolkman (1978) on siphons also indicate critical velocities in the range of 0.8 m/s.

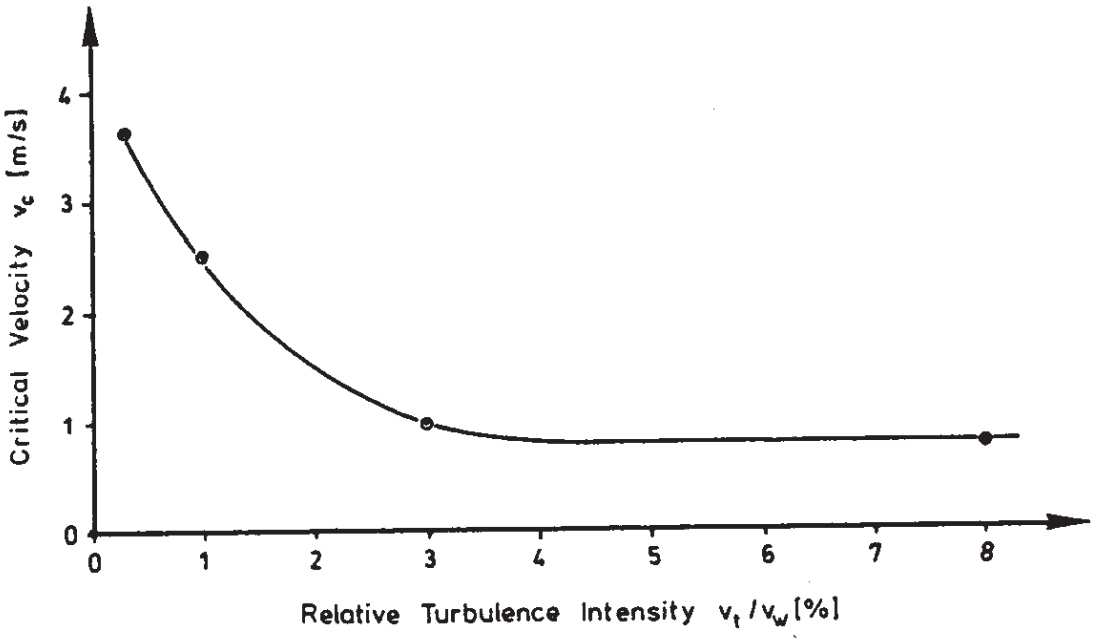


Fig. 2.1: The critical velocity for air entrainment in a plunging circular water jet (Ervine, 1980)

It must be noted that this discussion has excluded the case of the entrainment into a hydraulic jump. In this case in addition to the mechanism described above it is thought that the unsteady flow in the surface roller above the entering jet greatly contributes to the entrainment. The turbulence intensity and scale in the surface roller increases with increasing Froude number of the approach flow. At Froude numbers slightly larger than one, unbroken surface waves without air are observed. According to Henderson, 1971, the entrainment processes commence at Froude numbers larger than about 1.7.

Finally, for flows with a mean velocity parallel to the air-water surface as on a spillway there is no point of impingement and thus, although equation (2.4) still holds, the value of $v_c$ must be expected to be an order of magnitude larger than the values given above. From considerations of the turbulent characteristics of high speed flows, Ervine, 1985, comes to the conclusion that free surface aeration occurs when the turbulent fluctuations in eddies close to the surface reach values of 0.25 to 0.30 m/s in small eddies of 0.001 to 0.01 m in size.

## 2.4 Entrainment limit and entrained air flow rate

In the limiting case of fully turbulent flow (very high Reynolds numbers), one has to expect that the process of air entrainment will finally become independent of viscosity, since the large-scale turbulence is governed by inertial reactions alone. In these cases the amount of air entrainment, expressed either as total flow rate or as flow rate per per unit length of surface discontinuity, becomes

$$Q_{ae}, q_{ae} = f_{12}(v_e; \varrho_w; g) \tag{2.5}$$

This leads to a single dimensionless parameter, which hence must necessarily attain a constant value:

$$\frac{Q_{ae}}{v_e^5/g^2}; \frac{q_{ae}}{v_e^3/g} = \text{const}_{12} \tag{2.6}$$

and from this, with ($q_w = v_e \cdot y_e$) there follows

$$\frac{q_{ae}}{q_w} \equiv \beta_e = \text{const}\,\frac{v_e^2}{g y_e} = \text{const}\,Fr^2 = k_e\,Fr^2 \tag{2.7}$$

with $k_e$ defined as an "entrainment coefficient". In fully turbulent flow, $k_e$ should be constant for a given boundary geometry and hence the relative air entrainment should be directly proportional to the square of the local Froude number.

An example of air entrainment governed by this condition is shown in Figs. 2.2 and 2.3. Renner (1973) performed extensive experiments for the basic configuration of a jet impinging on an inclined wall. (This configuration is found e.g. in self-priming siphons with a deflector nose, in which the air entrainment observed here serves for evacuating the siphon hood). In the impingement region, a surface roller forms which entrains air (Fig. 2.2). The experimental results shown in Fig. 2.3 clearly confirm equation (2.7) over a wide range of Froude numbers; deviations from this relation are attributed to approaching the transport limit of the configuration.

In the general case, the viscosity $\mu_w$ and the turbulence characteristics Tu of the approach flow have to be added to the list of independent variables in equation (2.5). This results then in the following relation:

$$\beta_e = k_e\ (Re;\ Tu) \cdot Fr^2 \tag{2.8}$$

The factor Tu summarizes all relevant conditions of the approach flow which may be expected to have an influence on the mechanics of the entrainment process. This includes the velocity distribution over the cross section, flow curvature effects, turbulence intensity and -scale, and air content in the approach flow.

A different set of parameters, satisfying the condition that the air flux is zero when the velocity is less than the critical velocity, can be written as

$$\frac{Q_{a,e}}{(v-v_c)^5/g^2} = f\,(Re;\ Tu;\ Z) \tag{2.9}$$

For flows with large velocities, one can assume

$$\frac{v-v_c}{v} \approx 1 \tag{2.10}$$

and in this case the relationship (2.9) reduces again to the relationship (2.8).

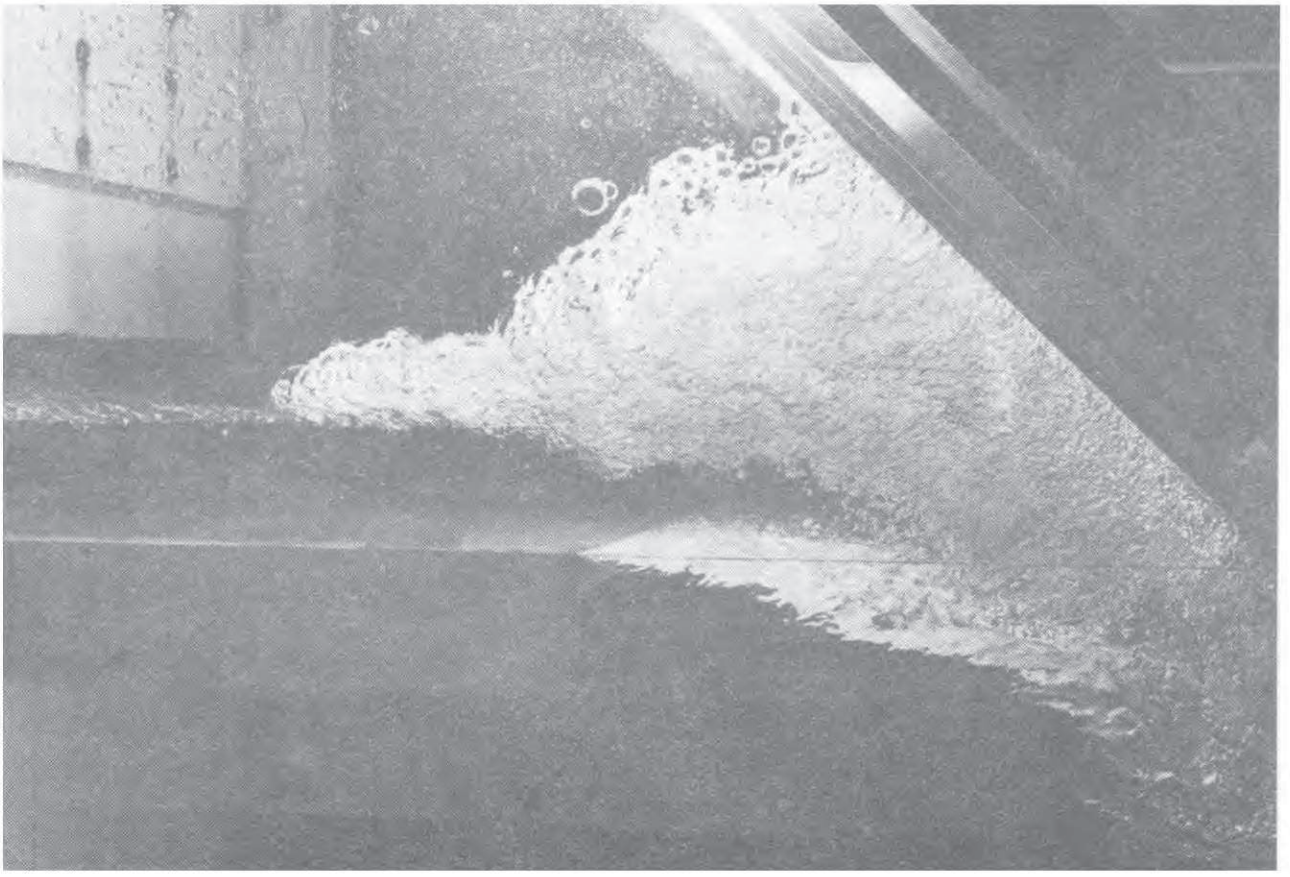

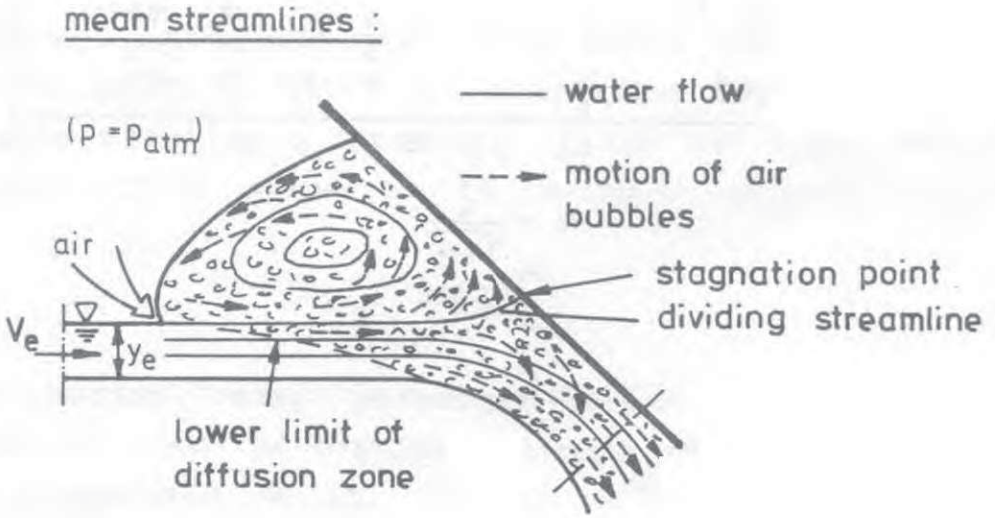


Fig. 2.2: Impinging jet configuration (Renner, 1973)

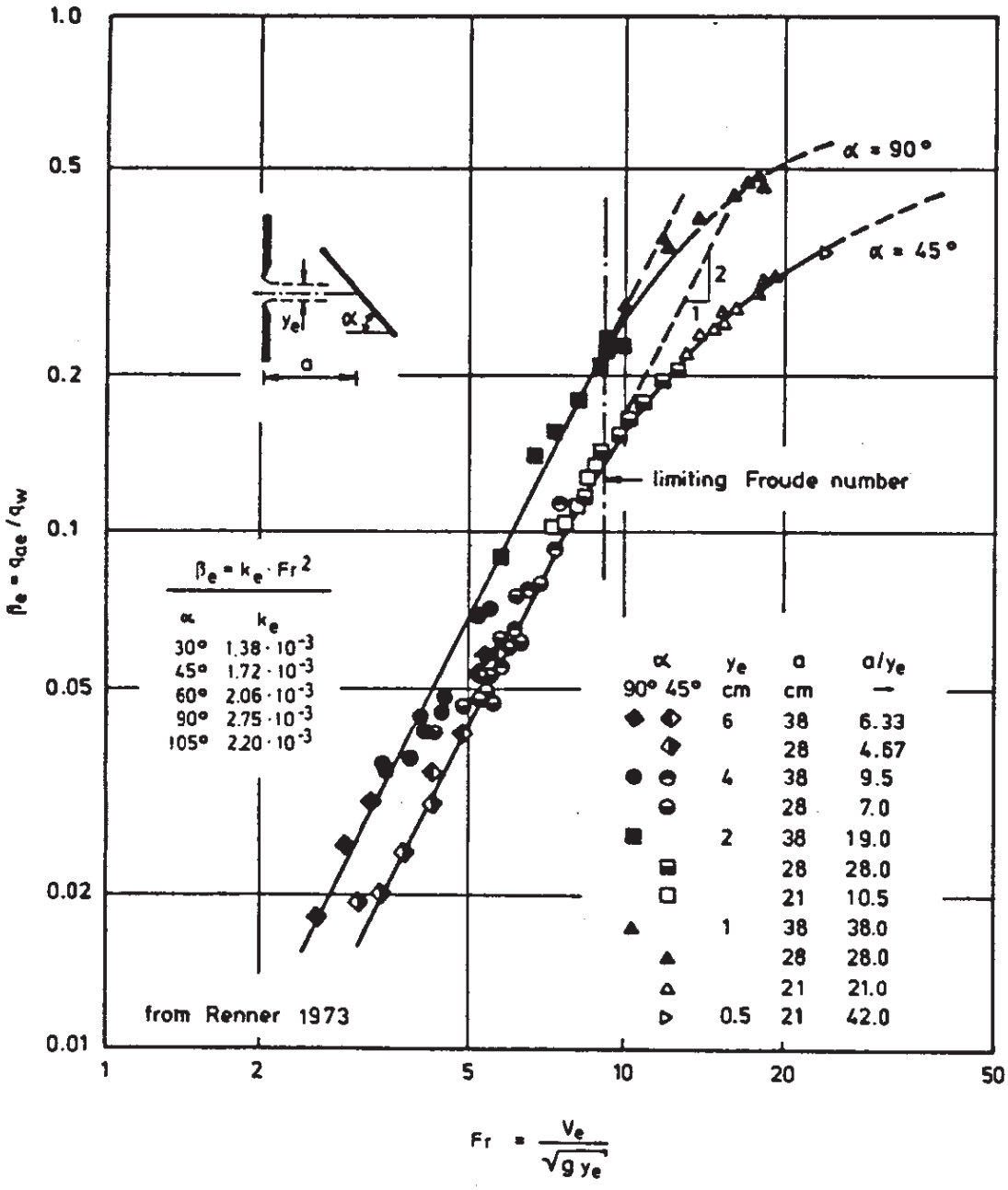


Fig. 2.3: Air entrainment in impinging jets: correlation of experiments with equation (2.7)

## 2.5 Weirs and drop structures

### 2.5.1 Critical velocity

Ervine's extensive investigations on the critical velocity for air entrainment in a plunging circular jet have led to the result shown in Fig. 2.1. Assuming that in technical applications the approach flow usually has a turbulence intensity of at least a few percent, one obtains for practical purposes a critical velocity of

$$v_c \approx 0.80 \text{ m/s} \qquad (2.11)$$

It seems permissible to assume that this value applies to any flow configuration of the plunging-jet-type, as long as the jet is still coherent at the point of impingement.

For jets with a great height of fall, air entrainment may commence in the free jet and the jet surface may desintegrate before it reaches the water surface. This has a strong effect on the air entrainment rate. Jet desintegration will occur when the turbulent shear layers have spread from the outer edge to the centerline of the jet and thus the inner core of the jet has decayed.

The distance $L_o$ from the weir plate along the centerline of the nappe to the point of total desintegration depends upon the flow rate and the turbulence intensity of the jet flow. For circular jets, Ervine (1980) quotes the following relationship by Baron:

$$\frac{L_o}{d_n} = 537.6 \frac{We}{Re^{5/8}} \qquad (2.12)$$

Ervine's experiments indicate the strong influence of the initial jet turbulence upon the distance $L_o$. In Fig. 2.4 his results are shown in comparison to Eq. (2.12). More recent experiments of Ervine, 1985, at larger scales confirm the result that for typical jet turbulence intensities of 3 to 8 % the relative breakup length $L_o/d_n$ is of the order of 50 to 100.

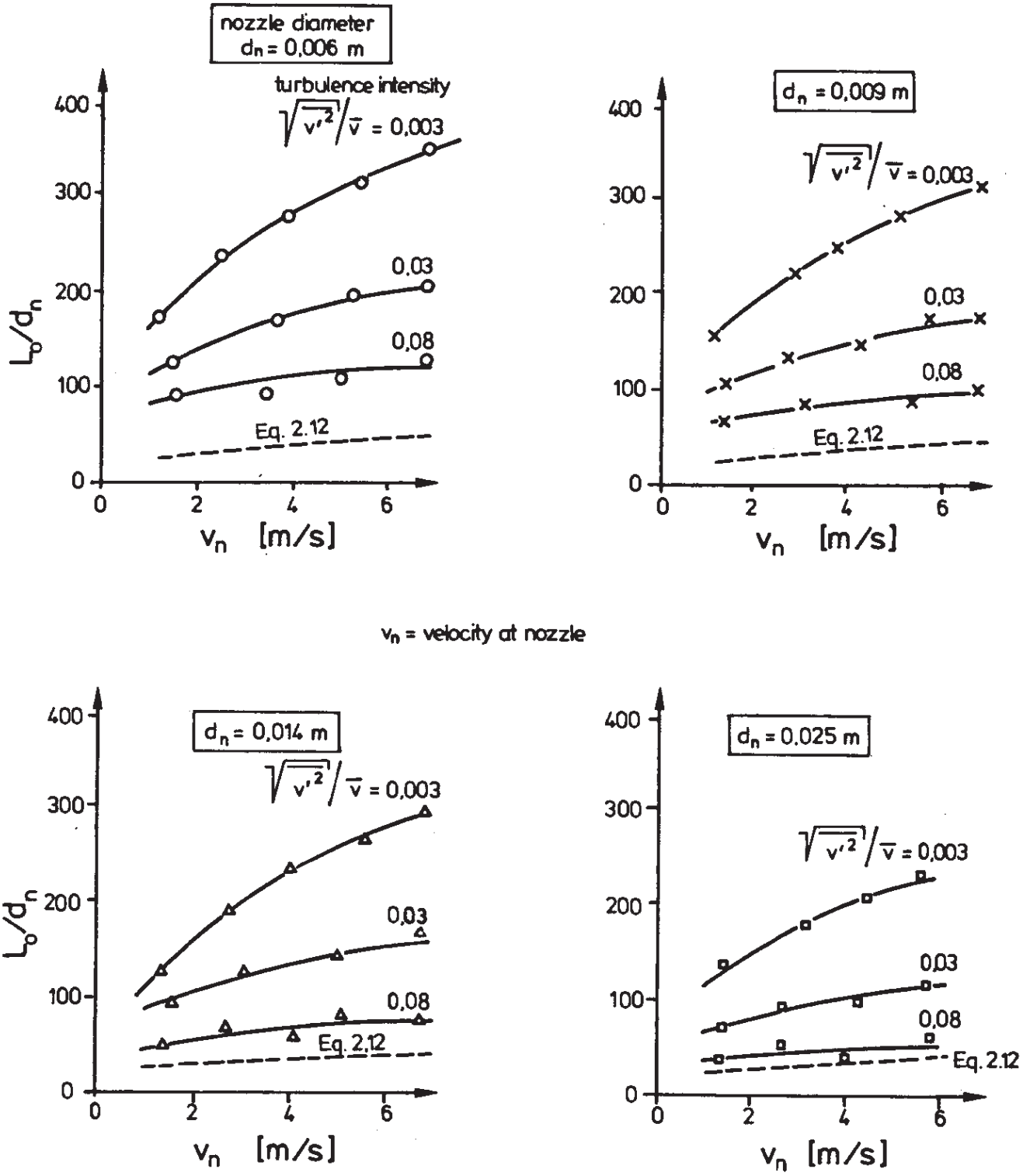


Fig. 2.4: Relative break-up length $L_o/d_n$ and jet velocity for circular nappes according to Ervine (1980)

For plane nappes, Avery (1976) quotes an investigation of Horeni (1956) which is plotted in Fig. 2.5. This relationship was visually confirmed by Avery. Outside the verified range, it may be useful for a first rough guess.

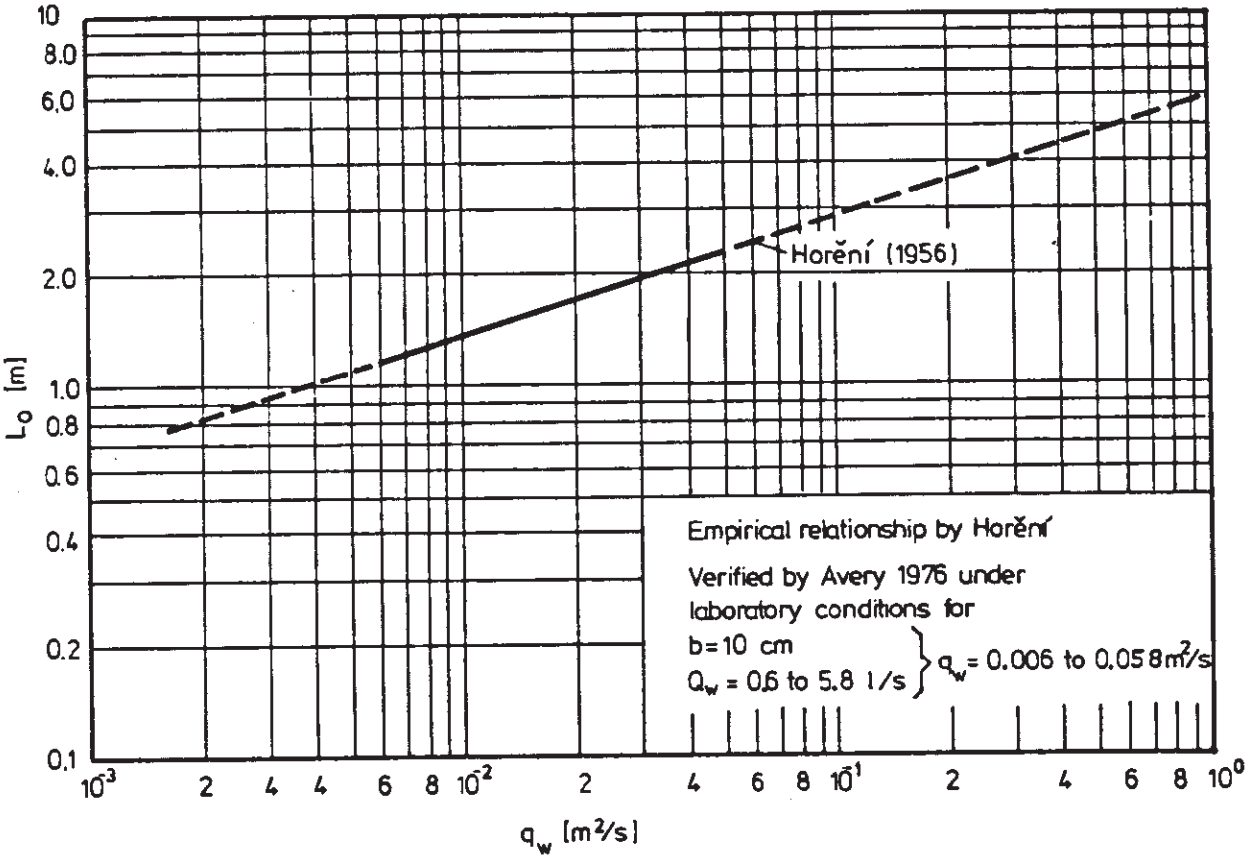


Fig. 2.5: Jet break-up length $L_o$ for plane nappes according to Avery (1976)

2.5.2 Air entrainment rate

For rectangular vertical drop shafts into which water is discharged in the form of a wall jet, Ervine (1980) has conducted numerous experiments over a wide range of conditions. The results are shown in Fig. 2.6. His experiments for air entrainment on one side of the jet can be summarized by a mean correlation function for the air discharge per unit width of the form (Ervine, 1981).

$$\beta = \frac{q_{a.e}}{q_w} = 0.0045\ Fr^2 \left(1 - \frac{v_c}{v_w}\right)^3 \quad \text{with} \quad v_c = 0.8\ m/s \qquad (2.13)$$

The bulk of the experimental data is within ± 20% of this relationship. Equation (2.13) then provides adequate design information based on the following parameter range:

| | |
|---|---|
| height of fall: | from 0.20 to 2.00 m |
| water velocities at the point of impact: | from 3.00 to 6.00 m/s |

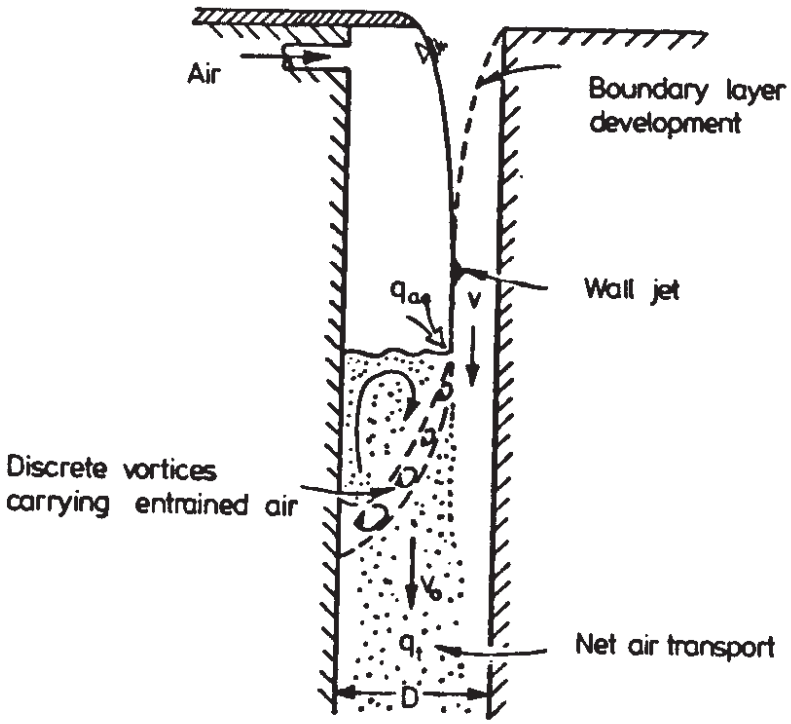


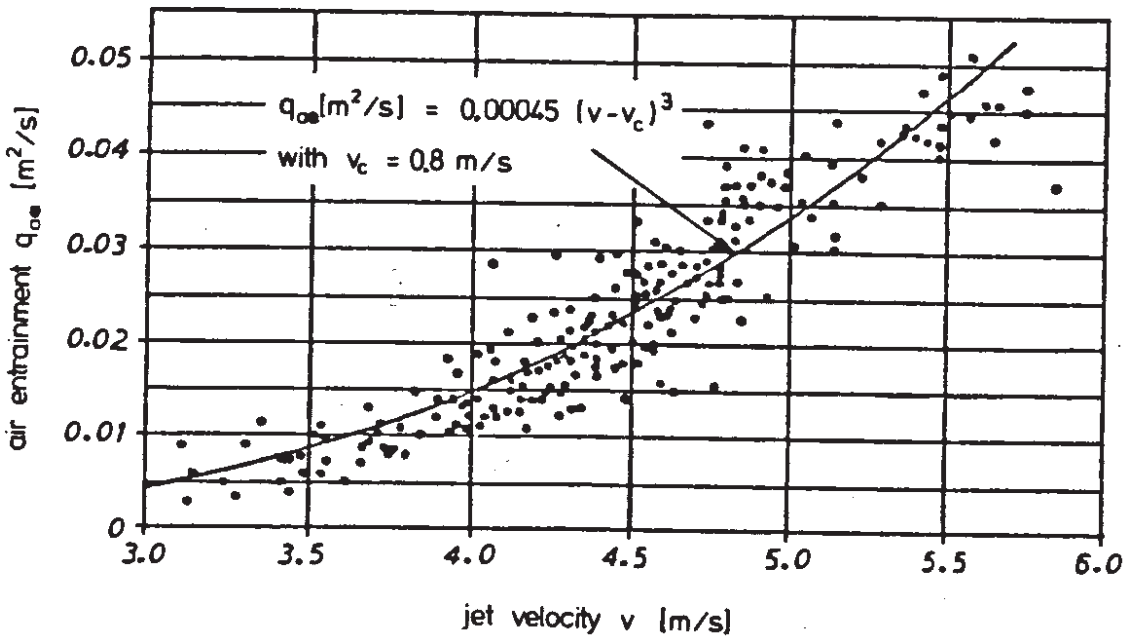


Fig. 2.6: Ervine's experiments on air entrainment in plunging jets or drop shafts

For the discharge over sharp-crested weirs, equation (2.13) may provide a reasonable estimate for wide rectangular weirs without aeration (i.e. air is entrained only on one side). For aerated weirs, air is entrained also under the nappe, so that the length of entrainment is doubled and hence also the air entrainment rate may be expected to double.

For sharp crested weirs of limited width or of a shape deviating from the rectangular form, the air entrainment may be expected to vary with the shape of the jet at the impingement cross section. The deformation of a free falling nappe has been studied by Avery and Novak (1978). They define a Froude number on the basis of the jet discharge per unit jet perimeter,

$$q_j = R\sqrt{2gh} \tag{2.14}$$

where R is the hydraulic radius of the jet at impact. With this, the jet Froude number is defined as

$$Fr_j = \frac{v}{\sqrt{gd}} = \left(\frac{\pi\sqrt{2gh^5}}{Q_w}\right)^{1/4} = \left(\frac{gh^3}{2q_j^2}\right)^{1/4} \tag{2.15}$$

Solid jets from a rectangular notch either converge fairly quickly to a circular cross section or diverge to flat rectangular shapes (Fig. 2.7). The criterion for a jet to diverge is

$$H/b > 1.288 \text{ : divergent} \qquad (2.16)$$
$$H/b < 1.288 \text{ : convergent}$$

and the height at which convergent jets become circular is given by the authors in dimensional form as

$$h\ [m] = 431\, b^{0.36}\ [m] \cdot Q_w^{0.8}\ [m^3/s] \tag{2.17}$$

The air entrainment rate $Q_{ae}$ can be assumed to be proportional to the total length p of jet surface intersection with the water surface, for wide rectangular jets, the intersection length p be-

comes twice the width B (B/p ≈ 1/2). For this case, Ervine and Elsawy (1975) give the following empirical relationship:

$$\beta \equiv \frac{Q_{ae}}{Q_w} = 0.13 \cdot \left(\frac{h}{d}\right)^{0.446} \cdot \left(1 - \frac{v_c}{v}\right) \qquad (2.18)$$

from experiments covering the following range:

| | | | |
|---|---|---|---|
| heigth of fall: | 0 | to 2.0 | m |
| water discharge: | 0 | to 0.1 | $m^3/s$ |
| jet width: | 0 | to 0.25 | m |
| jet thickness: | 0 | to 0.10 | m |
| jet velocity: | 0 | to 10 | m/s |

The minimum velocity to entrain air was found in these experiments to be approximately 1.1 m/s.

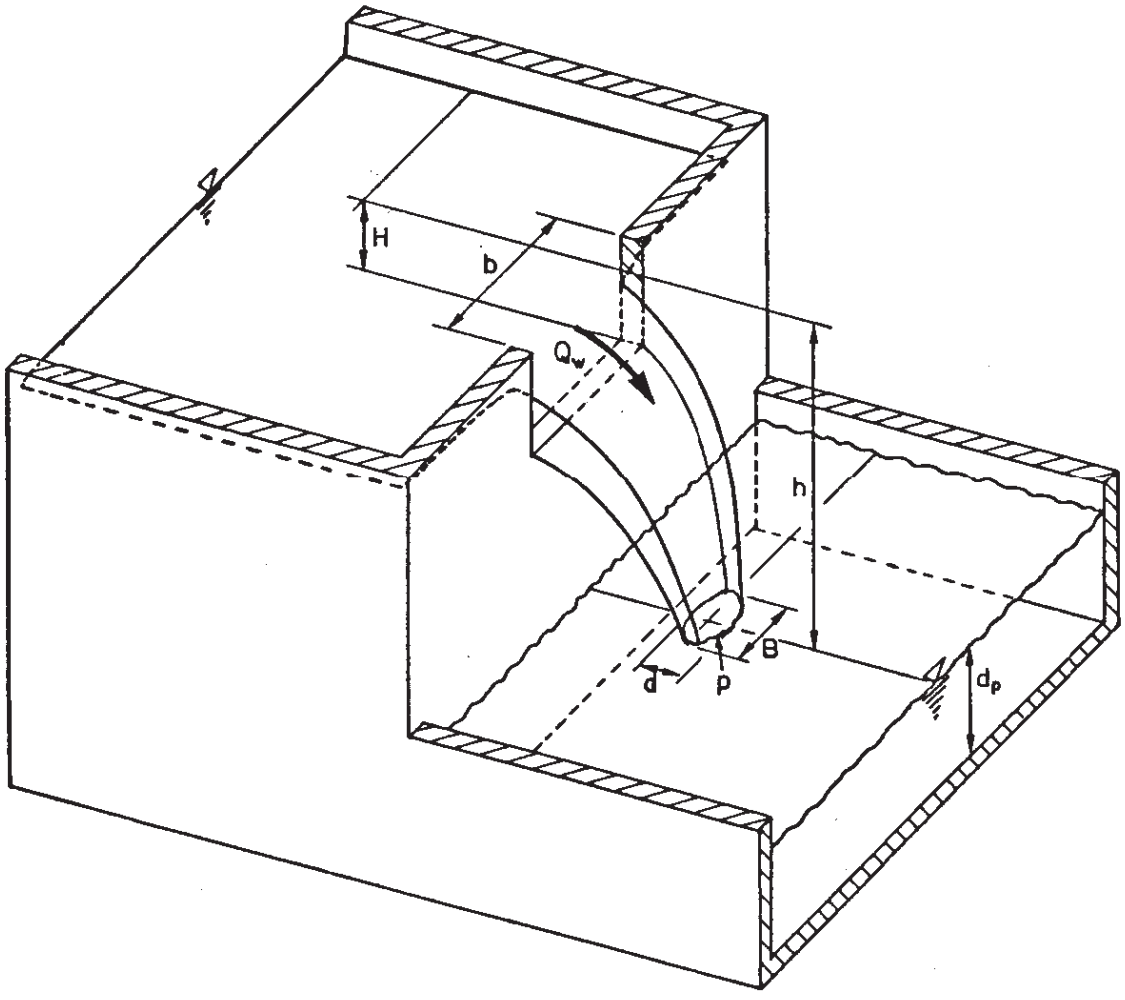


Fig. 2.7: Definition sketch for plane nappes falling from a rectangular notch

### 2.5.3 Oxygen transfer characteristics

For water quality purposes, local aeration processes are often welcome as means of increasing the oxygen content of the water. In these cases it is of interest to know the rate of mass transfer between air and water. This depends upon the concentration difference between air and water, upon the contact area, i.e. total surface area of the bubbles, and upon the surface renewal rate, i.e. turbulent mixing, contact times, and bubble trajectories. The process of reoxygenation can be considered in three consecutive steps:

- mechanics of air entrainment;
- mechanics of air transport away from the entrainment location, and
- transfer of oxygen from the air bubbles into solution.

The first two steps depend upon hydrodynamics alone, whereas the third step represents the phase of the process which depends upon the properties of the water, such as temperature, initial dissolved oxygen content, salinity, and degree of water pollution.

The bubble trajectory or residence time will be governed by the same parameters as the air entrainment. However, the turbulence characteristics (scale and intensity) of the flow and hence the Reynolds number may have a marked influence upon the bubble transport.

The mass transfer is described by the increase in concentrations in the water while passing the installation. For oxygenation, this is usually expressed in terms of the reoxygenation rate r in terms of oxygen concentrations c as follows:

$$r \equiv \frac{C_{Saturation} - C_{upstream}}{C_{Saturation} - C_{downstream}} = \frac{\text{deficit upstream}}{\text{deficit downstream}} \geq 1 \qquad (2.19)$$

This coefficient r will again depend upon the same parameters as the air entrainment rate, as well as upon the additional parameters governing the mass transfer rate, such as water tempera-

ture, water quality and pressure conditions. Therefore, when comparing results on mass transfer from various investigations, one has to reduce the data to "standard conditions" with respect to these parameters.

In general, standard conditions are considered to be given for
- atmospheric pressure
- water temperature of 15° C
- good water quality

Data reduction to this base is made by correction factors as follows. For temperature T, in degrees Celsius (from EPA, 1970):

$$f_T = \frac{(r-1)_T}{(r-1)_{15°C}} = \frac{1 + 0.046\,T}{1.69} \qquad (2.20)$$

For water quality:

$$f_{wq} = \frac{(r-1) \text{ given water quality}}{(r-1) \text{ base water quality}} \qquad (2.21)$$

with the following factors from WPR, 1973 for laboratory data and from Gameson, 1957 for field data:

| | $f_{wq1}$ (laboratory) | $f_{wq2}$ (field) |
|---|---|---|
| clean | 1.00 | -- |
| slightly polluted | 0.89 | 1.00 |
| moderately polluted | 0.56 | 0.81 |
| grossly polluted | 0.36 | 0.69 |

As one example of a generalized data presentation on the basis described above, Markofsky and Kobus (1978) have developed a diagram for sharp crested aerated rectangular weirs discharging into a deep plunging pool. In Fig. 2.8, all available model and field data are plotted, which describe in a consistent fashion the relation between observations at various scales. This figure clearly points out the effects of scale. However, the nomogram is

not intended for prediction of weir reoxyquation at a given location, and should not be used for predictions without proper caution and consideration of the restrictions (e.g. deep plunge pool) and uncertainties involved.

Novak points out that
- the plunge pool depth $d_p$ affects the oxygen uptake markedly since it affects the bubble trajectories, and
- that water quality and notably the salinity of the water have a significant effect on the mass transfer.

Novak gives an empirical correlation for the optimum depth $d_p$ of the downstream pool, which corresponds roughly to the maximum penetration depth of the air bubbles. This correlation is given in dimensional form as

$$d_p\ [m] = 0.00433 \cdot Re^{0.39} \cdot Fr_j^{0.24} \qquad (2.22)$$

At larger and at smaller plunge pool depths, the reoxygenation rate is less pronounced (Fig. 2.9).

For this optimum depth, Novak gives the following equations for the reoxygenation rate $r_{15}$ under standard conditions:

$$r_{15} - 1 = k_r\, Fr_j^{1.78}\, Re^{0.53} \qquad (2.23)$$

The coefficient $k_r$ is given as a function of the salinity (sodium nitrate) in the following form

| $NaNO_3$ | $k_r$ (-) |
|---|---|
| 0 % | $0.627 \cdot 10^{-4}$ |
| 0.3% | $0.869 \cdot 10^{-4}$ |
| 0.6% | $1.243 \cdot 10^{-4}$ |

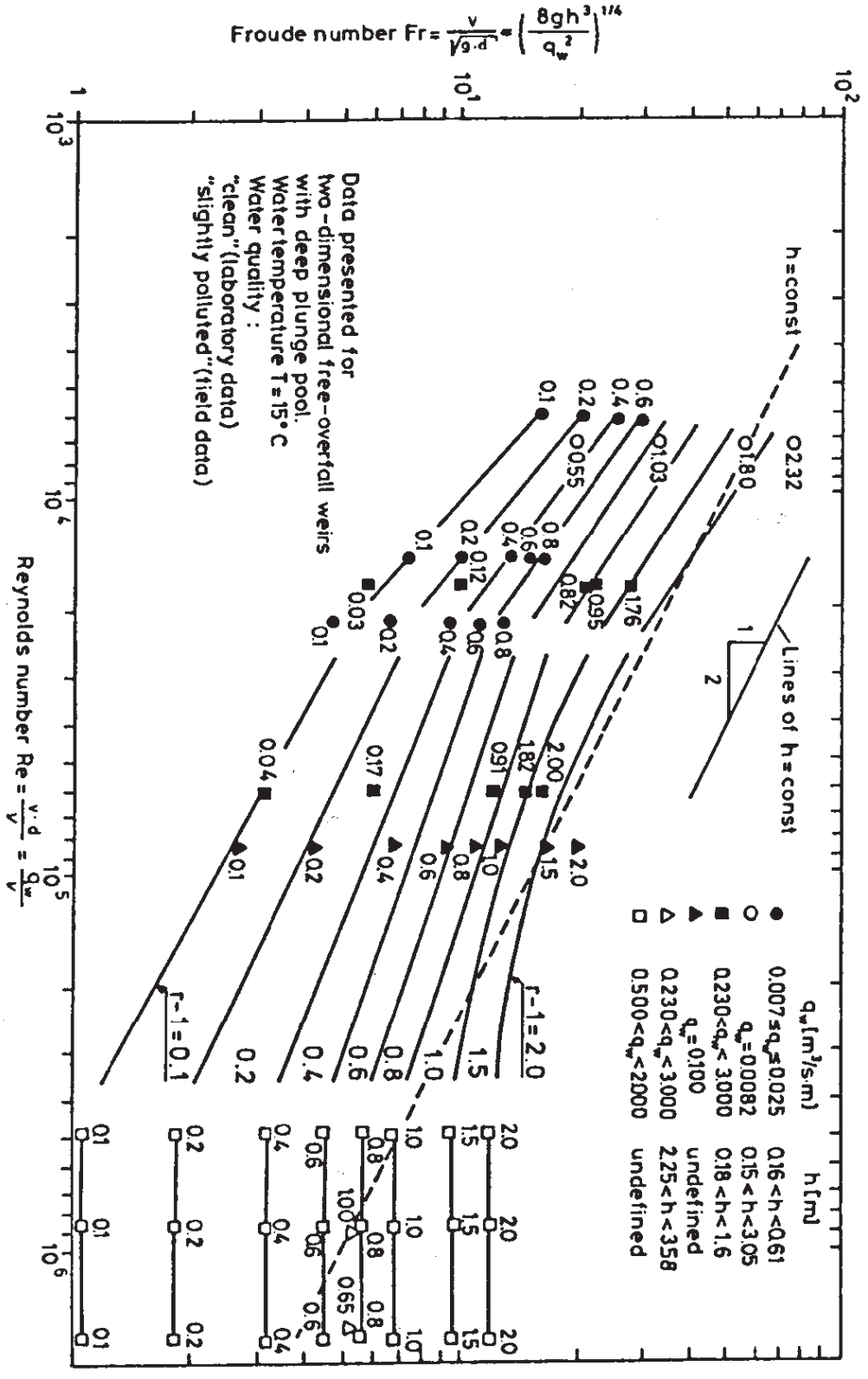


Fig. 2.8: Unified presentation of weir aeration data (rectangular weirs with deep plunge pools, Markofsky and Kobus, 1978)

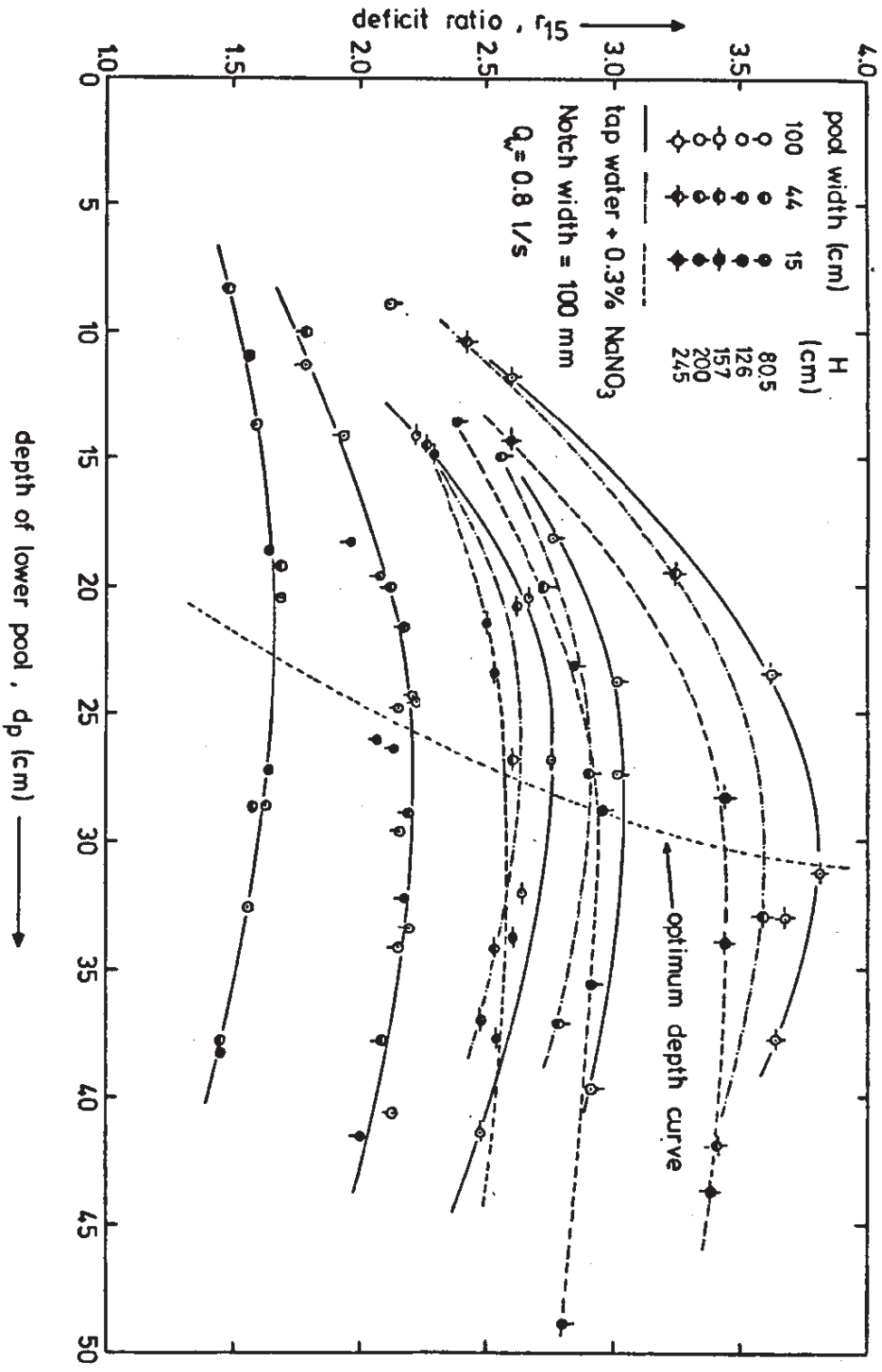


Fig. 2.9: The influence of plunge pool depth on the reoxygenation rate at weir structures (Novak, 1980)

A plot of equation (2.23) with available data over a wide range of discharges and heads as given in Fig. 2.10 shows good results.

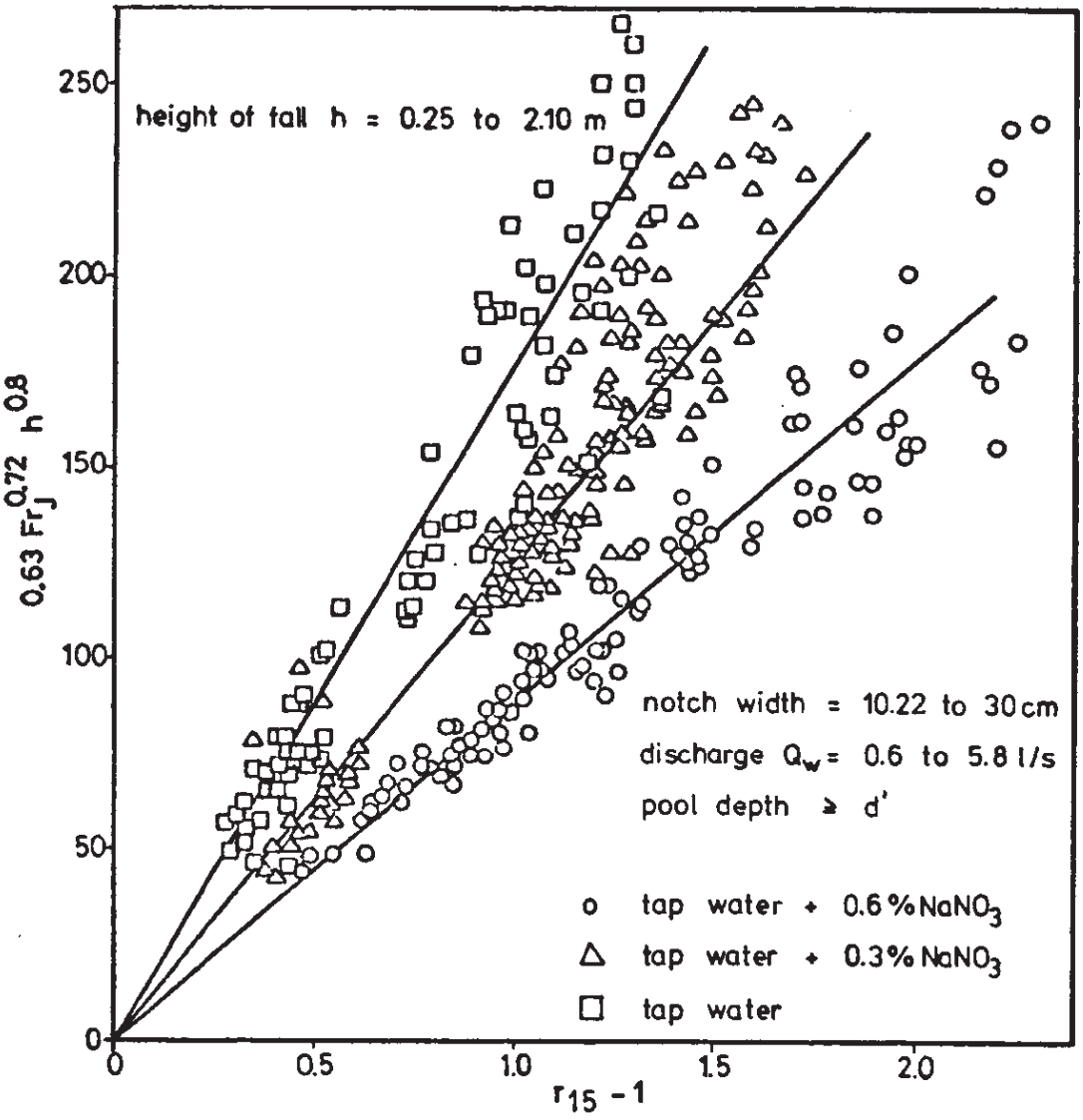


Fig. 2.10: Weir oxygenation: correlation of measurements with Equation 2.23 (Novak, 1980)

## 2.6 Hydraulic jump

Air entrainment in rectangular hydraulic jumps in open channels has been studied by Rajaratnam (1962), Resch and Leutheusser (1972) and Schröder (1963). Fig. 2.11 summarizes the experimental results.

Rajaratnam gives the relationship

$$\beta \equiv \frac{q_{ae}}{q_w} = 0.018\,(Fr-1)^{1.245} \qquad \text{(Fr from 2.5 to 9)} \qquad (2.24)$$

Renner gives the equation

$$\beta \equiv \frac{q_{ae}}{q_w} = 5\times10^{-3}\,Fr^2 \qquad \text{(Fr from 2.5 to 9)} \qquad (2.25)$$

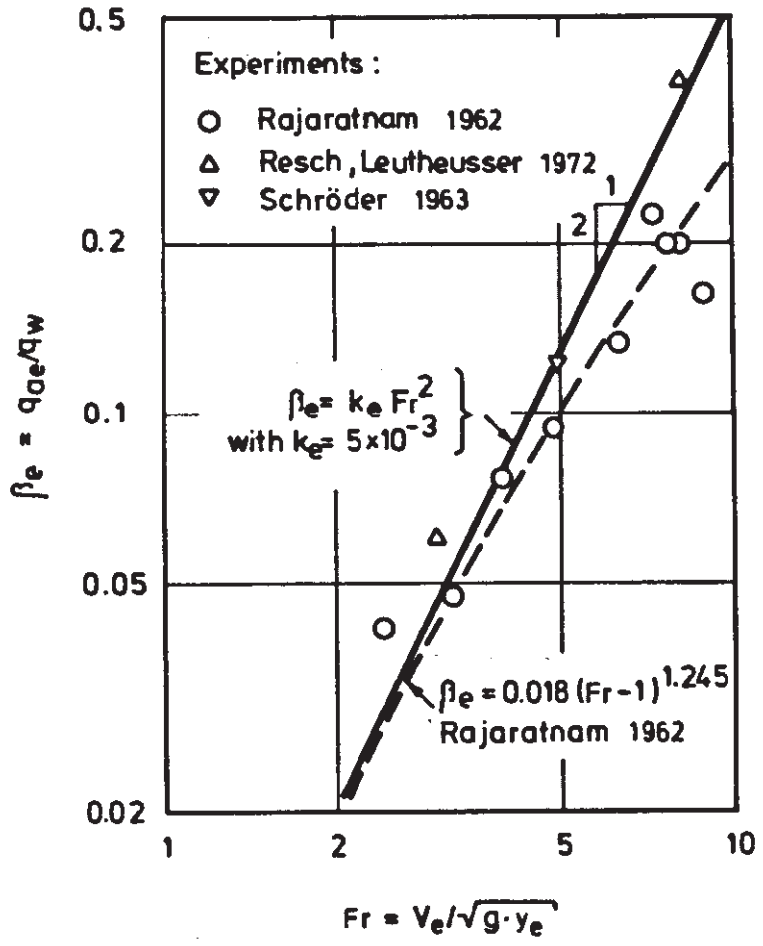


Fig. 2.11: Air entrainment in a hydraulic jump

As can be seen from Fig. 2.11, both relationships give a reasonable estimate for the entrainment at the toe of the hydraulic jump in the quoted range of Froude numbers. Comparison of both formulas for a given flow configuration gives an indication of the degree of uncertainty in the estimate of $q_{ae}$.

Information on the bubble sizes and on air concentrations in the flow has been given by Leutheusser and Resch (1973). Fig. 2.12 shows some experimental results which may be used as guideance for corresponding estimates.

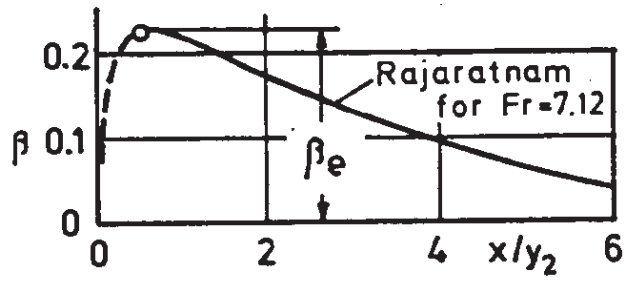


Void ratio distribution [%] for
Fr = 2,85 according to Leutheusser (1973)

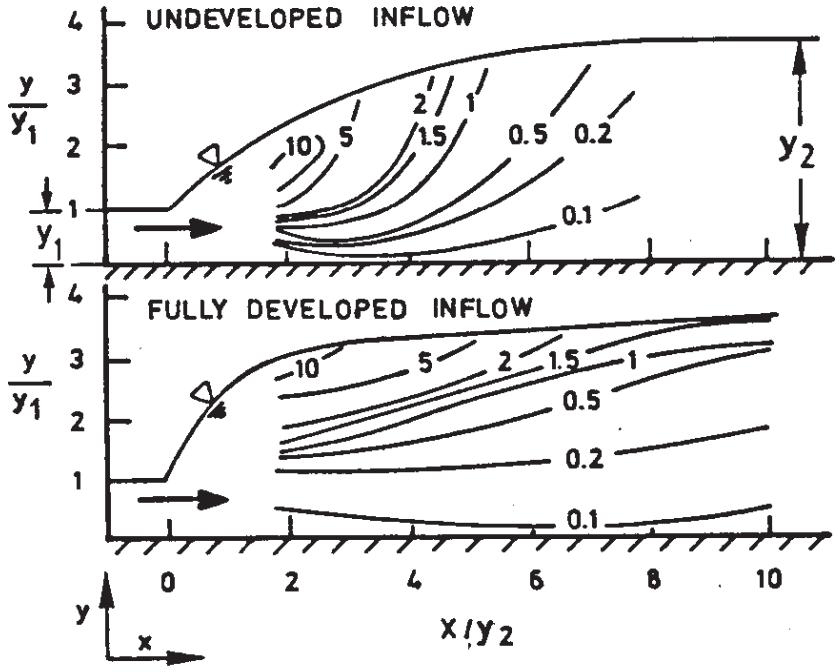


Fig. 2.12: Detrainment in a hydraulic jump

Mass transfer and oxygenation in hydraulic jumps have been investigated by Resch and Leutheusser (1974) and Novak et al. (1980). Novak has proposed the following correlation (see Fig. 2.13) for specific discharges experimentally verified in the range of 0.0146 to 0.0808 $m^2/s$:

$$r_{15} - 1 = k_1 \left(\frac{\Delta E}{y_1}\right)^{0.8} \left(\frac{q}{q_o}\right)^{0.75} \qquad (2.26)$$

with:

$\Delta E$ = energy head loss due to hydraulic jump
$q_o$ = 0.0345 $m^2/s$ (reference discharge)
$y_1$ = inflow water depth upstream of the hydraulic jump

and

| $NaNO_3$ | $K_1$ (-) |
|---|---|
| 0 % | 0.0158 |
| 0.3% | 0.0186 |
| 0.6% | 0.0230 |

It should be pointed out that numerous studies have investigated hydraulic jumps in closed conduits, leading from free-surface to pressurized flow. These studies cannot be compared directly to the free surface flow, because they may be strongly affected by the transport capacity of the pipe flow. This means that the measured entrainment rates reflect only the net transport capacity of the downstream conduit, which is controlling the process, and do not include the amount of air which is locally detrained again (difference between $q_{a,e}$ and $q_{a,t}$). Hydraulic jumps in closed conduits are treated in monograph A-12.

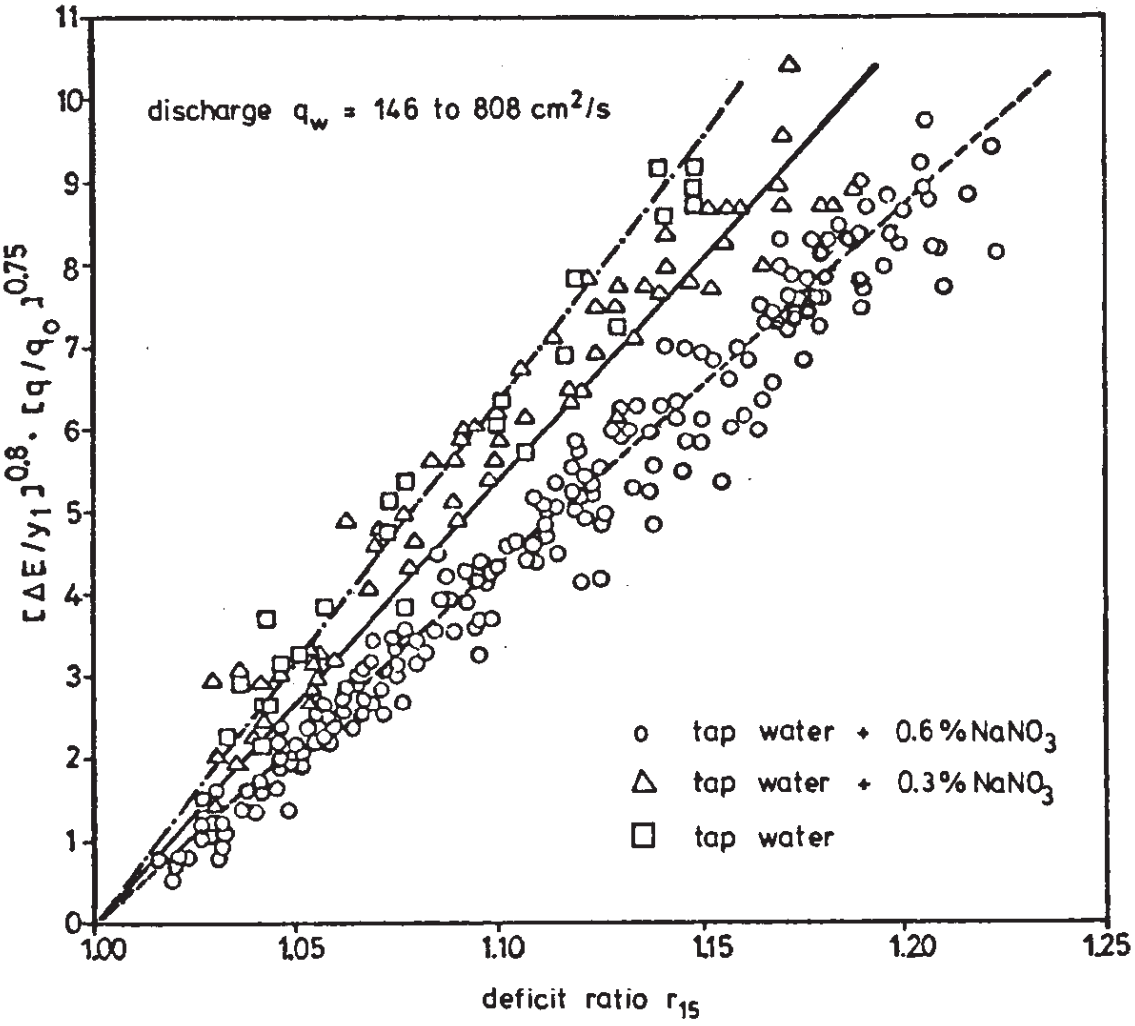


Fig.2.13: Oxygenation in hydraulic jumps: correlation of measurements with equation 2.26 (Novak, 1980)

## 2.7 Similarity considerations for hydraulic models

### 2.7.1 Modelling free surface flow with air entrainment

Studies of local air entrainment and detrainment rely heavily on experimental investigations on small scale models. Obviously, perfect dynamic similarity cannot be achieved, since the modelling parameters as derived from dimensional analysis cannot be satisfied simultaneously in a small scale model using the same fluids, i.e. air and water. It is often argued that the bubble sizes generated by free-surface aeration always exhibit about the same absolute size and hence violate in a small scale model both geometric similarity (ratio bubble size to boundary scale) and dynamic similarity (ratio of bubble rising velocity to water velocity).

Complete similarity requirements are described by equation (1.4). Restricting considerations to a small scale model of geometric similarity, using water of the same quality as in the prototype (i.e. Z = const) and entraining from the atmosphere (i.e. $c_{pe}=0$), this reduces to

$$\beta_e = f\,(Fr;\, Re;\, (Tu)) \qquad (2.27)$$

If according to the model law for free surface flows the Froude number is kept the same in model and prototype by proper choice of the model velocity scale, then the "scale effects" are embedded in the fact that the Reynolds number is not modelled correctly, and hence the turbulence characteristics (turbulence intensity, turbulent energy spectrum) of the flow. The parameter "Tu" stands for the turbulence characteristics of the approach flow in the inlet section of the model. Quite general, since the model Reynolds number is always smaller than the corresponding value of the prototype, the effects of viscosity are exaggerated in the small scale model.

However, in fully turbulent flow the mean flow characteristics and the turbulence macroscale structure become independent of the Reynolds number, since the energy transfer in turbulence production from mean flow to macroscale turbulent eddies is dominated by inertial effects and viscosity becomes apparent only in the small scale dissipation of turbulent energy. Under such conditions, the resulting scaling requirement is reduced to the requirement that in either case the Reynolds number must be large enough so that fully turbulent flow conditions prevail. In prototype, this condition is usually met, and therefore this requires simply

$$Re_{model} \geq Re_t \tag{2.28}$$

where $Re_t$ marks the minimum Reynolds number for fully turbulent flow. If the local values of water velocity and depth or thickness at the entrainment location are used, then it is surmised that the value of $Re_t$ is of the order of $10^5$. However, no definitive information about this value is available, and this limit may of course be different for different flow configurations. For instance, observations in plunging jets by Ervine, 1985, indicate that there may still be an influence of the Reynolds number at values well beyond the estimate given above.

In hydraulic models, the approach flow conditions at the inlet section of the model have to be prescribed. It has to be emphasized that not only the mean flow properties, but also the turbulence properties of the approach flow (as characterized by the parameter Tu) may have a very significant effect upon the air entrainment processes. This is well demonstrated by Fig. 2.4 and also known from other investigations, where by variation of the turbulence characteristics of the approach flow the entrainment characteristics were varied by as much as one order of magnitude. This stresses the point that for proper hydraulic modelling, reproduction of the approach flow conditions must include proper reproduction of the turbulence characteristics (Tu).

The scaling relationship equation (2.27) can be plotted, for given approach flow turbulence Tu, in general form as a graph of lines of constant $\beta_e$ in a Fr-Re plane. Such a diagram is sketched in Fig. 2.14, for which it should be noted that it comes from general similarity considerations and still requires verification by suitable experimental data. Since both Fr and Re are based on the same reference quantitites, lines of constant velocity and of constant reference lengths can be identified in this plane.

Information about the form of the relationship can be obtained from consideration of the asymptotic behaviour at the inception limit and the entrainment limit under fully turbulent conditions.

For "plunging-jet configurations" like weirs, drop structures and siphons, the inception limit is of importance. The relations of the form

$$q_{o,e} = k\,(v - v_c)^3 \qquad (2.29)$$

can be shown (see Thomas 1984) to imply

$$\frac{q_{oe}}{q_w} = k\,Fr^2\left(1 - \frac{v_c}{v}\right)^3 \qquad (2.30)$$

On the other hand, for "hydraulic-jump configurations" the entrainment limit is predominant. The relations of the general form

$$\beta_e = k_e\,(Fr - 1)^n \qquad (2.31)$$

approach in the limit the function

$$\beta_e = k_e\,Fr^2 \qquad (2.32)$$

The conditions of fully turbulent flow are reached when the local Reynolds number exceeds the value $Re_t$ as defined in equation (2.28). For Froude models, the following relationship for the

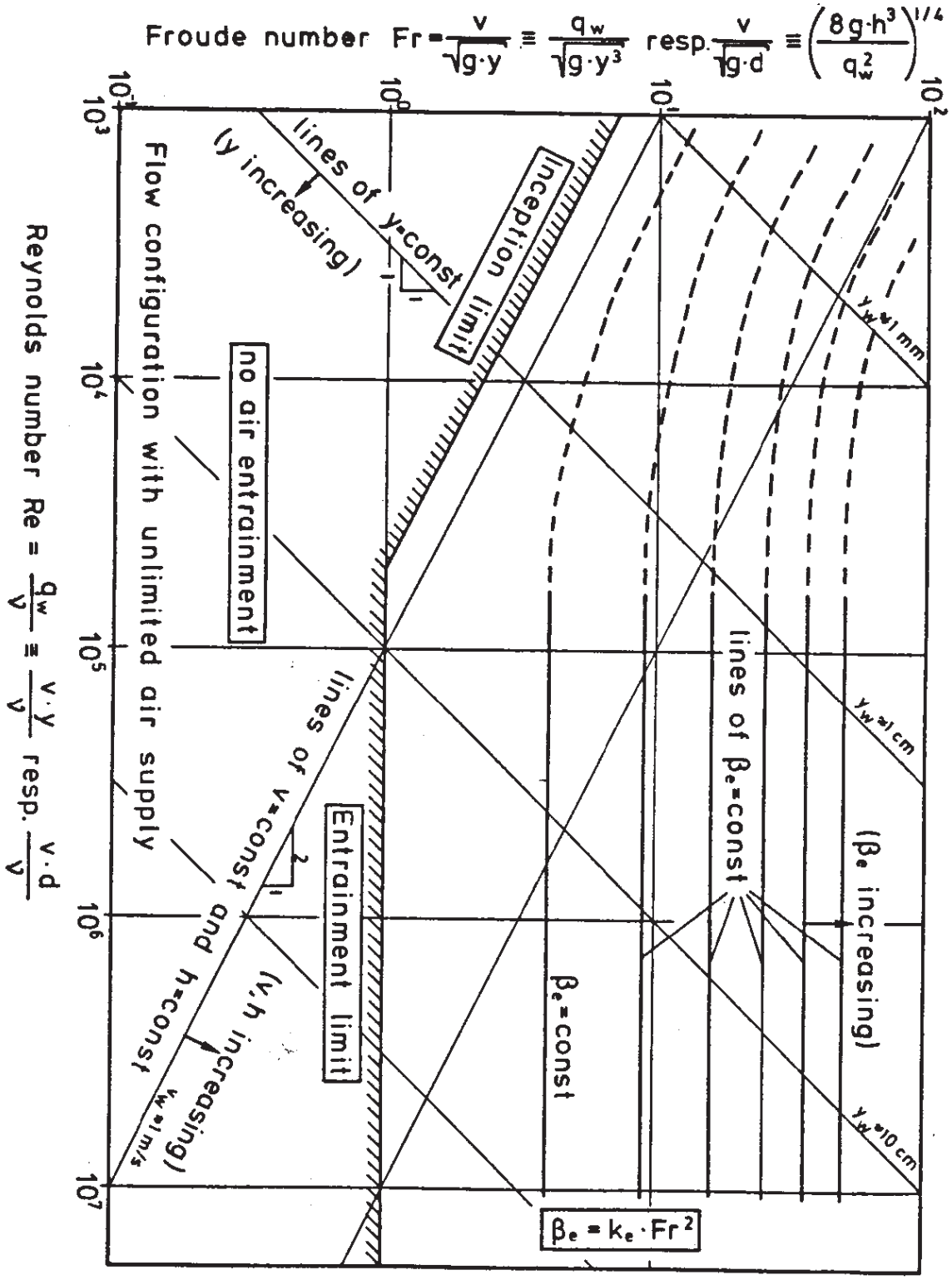


Fig. 2.14: Suggested functional relationship for the relative air entrainment (for given approach flow turbulence)

boundary length scale $l_e$ at the location of entrainment has been derived (Kobus, 1984):

$$l_e \geq \left[\frac{Re_t}{Fr}\left(\frac{\mu_w/\rho_w}{\sqrt{g}}\right)\right]^{2/3} \qquad (2.33)$$

For a given configuration, equation (2.33) allows an estimate of the model dimensions required for fully turbulent flow. This means, for instance, for models of hydraulic jumps with ($Fr_e > 1$), that equation (2.33) should be satisfied for the lower limit (Fr = 1) and hence necessarily also for all higher Froude numbers. This requires minimum water depths for critical flow of 10 cm for ($Re_t = 10^5$) and 2 cm for ($Re_t = 10^4$), respectively.

### 2.7.2 Additional criteria for similarity of air transport and escape

The question of transport and detrainment of air is closely linked to the question of the resulting bubble sizes. Since the resulting bubble size distribution depends upon the turbulence characteristics of the flow (and hence Reynolds number), the same is to be expected for the bubble transport and detrainment. The argument that in models bubble sizes are proportionally too large would hint at scale effects in the sense that detrainment is too large in the model and hence transport too small. This ties in with the fact that due to the lower turbulence level (smaller Reynolds number) the transport capacity in the model is expected to be smaller than in the prototype.

### 2.7.3 Additional conditions for similarity of oxygen transfer

Modelling mass transfer processes is even more uncertain due to the additional influence of the water quality. A discussion of Fig. 2.8 illustrates well the scaling considerations for plunging jets. In the laboratory, for low flow rates and low heights of fall (lower left corner), surface tension prevents air entrainment and therefore reoxygenation from occuring. The effect

of surface tension is overcome as a result of an increase in the flow rate or height of fall or both. Air is entrained to greater depths and, with increasing turbulence, is broken into finer and finer bubbles. Both effects increase the efficiency of the gas transfer process. Thus, in this region reoxygenation increases with both $q_w$ and h.

In the fully turbulent field situation, the amount of air entrainment is determined by the impingement velocity $v_e$ at the nappe which is a function of the height of fall h only. Thus, the same quantity of air will be entrained for the same height of fall regardless of the flow rate. Therefore, with increasing water flow rate, there is less air per volume of water available and thus the reoxygenation rate decreases. In the logarithmic parameter presentation, lines of constant h are given by straight lines with a slope of (- 1/2), i.e. parallel to the dashed line. Proceeding along such a line towards higher flow rates, i.e. to the right, shows that for a constant height of fall r decreases with increasing water discharge in the large- scale field situation. On the other hand, r increases with increasing height of fall at a given water flow rate (vertical line).

Considering small scale Froude models in Fig. 2.8, one proceeds along a horizontal line (Fr = constant) from left to right (to large Re) in going from a small scale Froude model to the prototype situation. It is seen that the reoxygenation rate r will necessarily be smaller in the model than in the prototype. Laboratory experiments for the determination of reoxygenation rates r have therefore often been performed at prototype dimensions of h. Historically, the results of such studies have been presented in equations in which r is a function of h only (see references in Markofsky and Kobus, 1978) without consideration of the flow rate $q_w$. Such equations will plot as straight lines with a slope of (- 1/2), i.e. parallel to the dashed line in Fig. 2.8, in these cases predictions of r from laboratory studies at low flow rates lead to overestimations of r for high flow rates at the same height of fall.

For any model study involving air entrainment, extreme care has to be taken that all parts of the flow configuration are modelled correctly, including the air supply system. It has been demonstrated e.g. by Thomas 1982 that even small changes in the geometry may greatly affect the air entrainment processes. For many problems, Froude models are adequate as long as the minimum model size as given by equation (2.33) is maintained.

REFERENCES

Avery, S.T., and Novak, P.: Oxygen Transfer at Hydraulic Structures. ASCE Journal Hy 11, November 1978.

Barczewski, B. Neue Meßverfahren für Wasser-Luftgemische und deren Anwendung auf zweiphasige Auftriebsstrahlen. Heft 45. Mitteilungen des Instituts für Wasserbau, Universität Stuttgart, 1979.

Brauer, H: Grundlagen der Einphasen- und Mehrphasenströmungen. Verlag Sauerländer, Aarau und Frankfurt am Main, 1971.

Comolet, R.: Sur le mouvement d'une bulle de gaz dans un liquide. La Houille Blanche, No. 1, pp. 31-42. 1979.

Davies, R.M., Taylor, G.I., Proc. Roy. Soc. (London), Vol. 200, Ser. A, pp. 375-390, 1950.

Environmental Protection Agency: Optimal Mechanical Aeration Systems for Rivers and Ponds. Water Pollution Control Research Series 16080 D007/70, 1970.

Ervine, D.A., Elsawy, E.M.: The Effect of a Falling Nappe on River Aeration. Proc. 16th IAHR Congress Sao Paulo, Brasil, 1975. (Paper C45).

Ervine, D.A.: The Entrainment of Air in Water. Water Power and Dam Construction. 28, No. 12, pp. 27-30, 1976.

Ervine A.: Scaling Relationship for a Two-Dimensional Vertical Dropshaft. Proc., BHRA Conference on Hydraulic Modelling of Civil Engineering Structures. Coventry, England. September 1982.

Ervine, A.: Two-phase Flow in Hydraulic Structures, Lecture Notes presented to the US Bureau of Reclamation, July 1985 (unpublished).

Ervine, D.A., McKeogh, E., and Elsawy, E.M.: Effect of Turbulent Intensity on the Rate of Entrainment by Plunging Water Jets. Proc. Instn. Civ. Engrs., Part 2. June 1980; pp. 425-455.

Falvey, H.T.: Air Water Flow in Hydraulic Structures. Water Resources Techn. Publication. Engineering Monograph No. 41. US Department of Interior. 1980.

Gameson, A. L. H.: Weirs and Aeration of Rivers. Journal of the Institute of Water Engineers, London, England, Vol. 11, 1957, pp. 477-490.

Goldring, B.T., Mawer, W.T., and Thomas, N.H.: Level Surges in the Circulating Water Downshaft of Large Generating Stations. Proc. BHRA Third International Conference on Pressure Surges, Canterbury, England, 1980.

Haberman, W.L., Morton, R.K.: David Taylor Model Basin, Report 802, 1953.

Haberman, W.L., Morton, R.K.: An Experimental Study of Bubbles Moving in Liquids. Proceedings ASCE. Vol. 80. pp. 379-427,1954.

Henderson, F.M.: Open Channel Flow. McMillan Co., New York, 1971.

Hino, M.: On the Mechanism of Self-Aerated Flow on Steep Slope Channels, Application of the Statistical Theory of Turbulence. International Association of Hydraulic Research, Ninth Convention, Dubrovnik, Yugoslavia, pp. 123-132. 1961.

Horenî, P.: Disintegration of a Free Jet of Water in Air. Vyzkumny Ustav Vodohospodarsky Prace a Studie, Sesit 93, Praha-Podbaba, 1956.

Kobus, H.: Bemessungsgrundlagen und Anwendungen für Luftschleier im Wasserbau. Heft 7. Schriftenreihe "Wasser und Abwasser in Forschung und Praxis", Erich Schmidt Verlag. Berlin, 1973.

Kobus, H.: Local Air Entrainment and Detrainment. Proc. IAHR Symposium on Scale Effects in Modelling Hydraulic Structures. Esslingen, Germany, September 1984.

Kobus, H., Westrich, B.: An Example of a Combined Discharge-Control and Aeration Structure. Prox. XX. Congress IAHR. Moscow, USSR. September 1983.

Lane, E.W.: Eintrainment of Air in Swiftly Flowing Water. Civil Engineering 9, No. 2, pp. 88-91, 1939.

Leutheusser, H.J., Resch, F.J., and Alemu, S.: Water Quality Enhancement Through Hydraulic Aeration. Proc. 15th Congress IAHR, Istanbul, Turkey, September 1973.

Markofsky, M., and Kobus, H.: Unified Presentation of Weir-Aeration Data. ASCE Journal of Hydraulic Research, April 1978.

Novak, P.: Luftaufnahme und Sauerstoffeintrag an Wehren und Verschlüssen. In: DVWK Schriftenreihe "Natur- und Modell-messungen zum künstlichen Sauerstoffeintrag in Flüssen". Heft 49. Paul Parey Verlag. Hamburg, 1980.

Rajaratnam, N.: An Experimental Study of Air Entrainment Characteristics of the Hydraulic Jump. Journal of the Institution of Engineers of India. Vol. 42. No. 7. March 1962.

Rajaratnam, N.: Hydraulic Jump. Advances in Hydroscience, 4, Ed, Ven T. Chow, Academic Press, New York and London, pp. 255-262, 1967.

Resch, F.J., Leutheusser, H.J.: Le ressaut hydraulique: mesures de turbulence dans la région diphasique. La Houille Blanche, Vol. 27, No. 4, 1972, pp. 279-294.

Resch, F.J., Leutheusser, H.J., and Alemu, S.: Bubble Two-Phase Flow in Hydraulic Jump. Journal of the Hydraulic Division ASCE, Vol. 100, No HY1, January 1974.

Renner, J.: Lufteinmischung beim Aufprall eines ebenen Wasserstrahls auf eine Wand. Dissertation. Universität Karlsruhe. 1973.

Schröder, R.: Die turbulente Strömung im freien Wechselsprung. Mitteilungen. Institut für Wasserbau und Wasserwirtschaft. TU Berlin, Heft 59. 1963.

Thomas, N.H.: Research Report to CEGB. Department of Applied Mathematical and Theoretical Physics, Cambridge, 1978.

Thomas, N.H.: Air Demand Distortion in Hydraulic Models: Experimental Evidence of Bi-Modal Structure in Air Entraining Flows and a Scaling Analysis of Detrainment with Special Applications to Siphon Priming. Proc. BHRA Conference on Hydraulic Modelling of Civil Engineering Structures, Coventry, England, September 1982.

Thomas, N.H., Auton, T.R., Sene, K. and Hunt, J.C.R.: Entrapment and Transport of Bubbles in Large Eddies in Multiphase Turbulent Shear Flows. International Conference on the Physical Modelling of Multiphase Flows, BHRA, Coventry, 1983.

Volkart, P.: The Mechanism of Air Bubble Entrainment in Self-Aerated Flow. Int. J. Multiphase Flow, 6, pp 411-423, 1980.

Water Pollution Research Laboratory, England, Aeration at Weirs. Notes on Water Pollution, No. 61, June, 1973.

Wood, I.R.: The Uniform Region in Self-Aerated Flow. Proc. ASCE Hydraulic Division. Vol. 109. No. 3. March 1983.